The Intestinal Nuclear Receptor Signature With Epithelial Localization Patterns and Expression Modulation in Tumors

SALVATORE MODICA,[*] FRANCOISE GOFFLOT,[‡] STEFANIA MURZILLI,[*] ANDRIA D'ORAZIO,[*] LORENA SALVATORE,[*] FABIO PELLEGRINI,[§,‖] ANTONIO NICOLUCCI,[§] GIOVANNI TOGNONI,[§] MASSIMILIANO COPETTI,[‖] ROSA VALANZANO,[¶] SERENA VESCHI,[#] RENATO MARIANI–COSTANTINI,[#] GIUSEPPE PALASCIANO,[*] KRISTINA SCHOONJANS,[**] JOHAN AUWERX,[‡,**] and ANTONIO MOSCHETTA[*]

[*]Department of Translational Pharmacology, [§]Department of Clinical Pharmacology and Epidemiology, Consorzio Mario Negri Sud, Santa Maria Imbaro, Chieti, Italy, and Clinica Medica Murri, University of Bari, Bari, Italy; [‡]Institut Clinique de la Souris, CNRS/INSERM, Université Louis Pasteur, Illkirch, France; [‖]Unit of Biostatistics, IRCCS "Casa Sollievo della Sofferenza," San Giovanni Rotondo, Foggia, Italy; [¶]Department of Clinical Physiopathology, University of Florence, Florence, Italy; [#]Unit of Molecular Pathology and Genomics, Center for Sciences on the Ageing (CeSI), "Gabriele D'Annunzio" University Foundation and Department of Oncology and Neurosciences, Chieti, Italy; and [**]Ecole Polytechnique Fédérale de Lausanne, Lausanne, Switzerland

BACKGROUND & AIMS: The WNT–adenomatous polyposis coli system controls cell fate in the intestinal epithelium, where compartment-specific genes tightly regulate proliferation, migration, and differentiation. Nuclear receptors are transcription factors functioning as sensors of hormones and nutrients that are known to contribute to colon cancer progression. Here we mapped the messenger RNA (mRNA) abundance and the epithelial localization of the entire nuclear receptor family in mouse and human intestine. **METHODS:** We used complementary high-resolution in situ hybridization and systematic real-time quantitative polymerase chain reaction in samples of normal distal ileum and proximal colon mucosa and tumors obtained from mouse and human adenomatous polyposis coli–initiated tumor models (ie, $Apc^{Min/+}$ mice and familial adenomatous polyposis patients) and in cellular models of human colon cancer. **RESULTS:** We first defined for each receptor an expression pattern based on its transcript localization in the distal ileum and the proximal colon. Then, we compared the mRNA levels between normal intestinal epithelium and neoplastic intestinal tissue. After analyzing the correspondence between mouse and human tumor samples plus genetically modified human colon cancer cells, we used complementary graphic and statistical approaches to present a comprehensive overview with several classification trees for the nuclear hormone receptor intestinal transcriptome. **CONCLUSIONS: We defined the intestinal nuclear hormone receptor map, which indicates that the localization pattern of a receptor in normal intestine predicts the modulation of its expression in tumors. Our results are useful to select those nuclear receptors that could be used eventually as early diagnostic markers or targeted for clinical intervention in intestinal polyposis and cancer.**

The intestinal epithelium is subdivided into anatomic units: in the crypt, stem cells generate proliferative precursors that progress into differentiated enterocytes lining the villus. Cellular positioning guarantees intestinal epithelium homeostasis and depends on cellular proliferation, migration, and differentiation along the crypt-villus axis. This process is driven by the *Wnt* signaling pathway.[1] Under normal conditions, stem cells give rise to proliferative progenitors, which have an activated *Wnt* signal that results in the inhibition of the adenomatous polyposis coli (APC) destruction complex able to phosphorylate and degrade β-catenin. Thus, in these proliferative cells at the bottom of the crypt, nuclear β-catenin is associated with members of the T-cell transcription factor family, activating the transcription of numerous genes that drive the proliferative phenotype.[2] Germline mutations of the *APC* gene are responsible for familial adenomatous polyposis (FAP),[3] a disorder in which patients present with a large number of colon polyps early in life with a high risk of developing colorectal cancer (CRC) after additional somatic mutations.[4–6] The fine-tuning of specific compartment-related transcription fac-

Abbreviations used in this paper: APC, adenomatous polyposis coli; AR, androgen receptor; CAR, constitutive androstane receptor; CKI, casein kinases I; COUP-TF, Chicken ovalbumin upstream promoter-transcription factor; CRC, colo-rectal cancer; DAX-1, Dosage-sensitive sex reversal-adrenal hypoplasia congenita critical region on the X chromosome, gene 1; ER, estrogen receptor; ERR, estrogen-related receptor; FAP, Familial Adenomatous Polyposis; FXR, farnesoid X receptor; GCNF, germ cell nuclear factor; GR, glucocorticoid receptor; GSK3β, glycogen synthase kinase 3β; HNF, hepatocyte nuclear factor; KLF4, Krüppel-like factor 4; LRH-1, liver receptor homolog 1; LXR, liver X receptor; MR, mineralocorticoid receptor; NGFIB, neuronal growth factor 1B; NOR1, neuron-derived orphan receptor 1; NR, nuclear receptors; QPCR, quantitative real-time PCR; PNR, photoreceptor-specific nuclear receptor; PPAR, peroxisome proliferator-activated receptor; PR, progesterone receptor; PXR, pregnane X receptor; RAR, retinoic acid receptor; ROR, RAR-related orphan receptor; RXR, retinoid X receptor; SF1, steroidogenic factor 1; SHP, small heterodimer partner; TCF-4, T-cell factor 4; TF, transcription factors; TLX, human homologue of the drosophila tailless gene; TR, thyroid receptor; TR2, 4, testicular receptor 2, 4; VDR, vitamin D receptor.

© 2010 by the AGA Institute
0016-5085/10/$36.00
doi:10.1053/j.gastro.2009.09.060

tors drives both the process of intestinal epithelium cell migration and differentiation as well as the neoplastic transformation.[5]

Nuclear receptors (NRs), one of the largest family of transcription factors with 48 members in human beings and 49 in mice,[7] are potential modulatory factors that influence the development of CRC. In fact, the NR family comprises the classic NRs for endocrine steroids such as corticoids, androgens, and estrogens, as well as receptors for fat-soluble vitamins E and D and fatty acids, bile acids, and several others lipids derived from the diet.[8,9] For a few NRs, termed *orphan NRs*, no endogenous ligands are as of yet known. NRs induce transcriptional activation of their target genes after recruiting co-activators in a ligand-dependent or ligand-independent manner.[10] Several studies have underscored the importance of NRs in the control of diverse homeostatic processes ranging from the regulation of reproduction, metabolism, and immunity.[11] A variety of NRs also directly regulate the cell cycle, mitosis, proliferation, and apoptosis.[12,13] Recently, NRs have been clustered in different classes based on their expression patterns in normal mouse and human samples.[14–18] The development of a functional NR atlas is a validated strategy to elucidate the entire program of NR structure, function, and role in disease with enormous therapeutic potential.[19] The aim of the present study was to provide a systematic analysis of NR localization and expression modulation in normal intestine and CRC.

By using complementary high-resolution in situ hybridization (ISH)[16] and systematic real-time quantitative polymerase chain reaction (RTqPCR),[14,15] we map the NR expression patterns in normal human and mouse intestine. Based on this work, and using cellular, mouse, and human models of CRC, as well as computational tools, we cluster the NR family into different quantitative expression and qualitative cell-type–specific networks. Our findings paint a unique picture of NR transcriptome from the normal intestine to the development of CRC. This resulting map of intestinal NRs offers guidance by bridging intriguing NR expression patterns with (patho)-physiological responses and eventually may lead to the more rational design of new approaches targeting NRs for the clinical management of CRC.

Materials and Methods

Patients

Ten unrelated Italian patients with FAP (5 females, 5 males; mean age, 24.5 y; range, 14–39 y) were recruited for the study after approval by the Ethical Committee of the University "G. D'Annunzio" of Chieti. Written informed consent was obtained from each patient. The 10 patients presented with a clinical diagnosis of FAP with histomorphologic confirmation of colonic adenomas and with a characterized germline mutation in the *APC* gene. Two APC mutations were diagnosed among the entire patient group (c.2527_2530 AGTT p.Ser843fsX860 and c.3927_3931 AAAGA p.Glu1309fsX1312), and no relevant differences for the present expression-profiling study could be detected on the basis of this germline characteristic.

Cell Lines

Stable transfected APC-inducible HT29 cells were obtained from Drs K. W. Kinzler and B. Vogelstein and were cultured as previously described.[20]

Animal Experiments

All experiments were performed on age- and sex-matched mice. The wild-type and $Apc^{Min/+}$ mice[21] were on a pure C57BL/6 background and were back-crossed more than 10 generations. Mice were housed in a temperature-controlled environment with 12-hour light/dark cycles and fed standard rodent chow diet ad libitum. All the experiments were conducted in male mice 12 weeks of age after a 4-hour fasting period, and the samples were collected between 8 and 10 AM. The entire set of analysis for this study was performed on distal ileum and proximal colon.

Nonradioactive High-Resolution ISH

Semiquantitative gene expression via ISH was detected with digoxigenin-labeled RNA probes (Supplementary Table 1), using 2 different methods (ie, manual and automated), using a Tecan robot (Männedorf, Switzerland).[16] Annotation was performed for mouse ileum and colon, with each region being assigned a pattern of expression as follows: ubiquitous, U; crypt, C; and villus, V, for the ileum and ubiquitous, U; crypt, C; or upper third of the crypt-epithelial surface, E, for the colon. For NRs with a gradient distribution between U and C, the final allocation was decided on the basis of signal intensity (Supplementary Table 2). Results were based on 3 hybridizations and 3 independent observers scored the signals.

RNA Preparation and RTqPCR Analysis

RNA was extracted from tissues and cells using TRIzol Reagent (Invitrogen, Carlsbad, CA). RTqPCR primers were designed using Primer Express Software (Applied Biosystems, Foster City, CA). Human and mouse NR primer sequences are available on request. RTqPCR reactions contained 60 ng of complementary DNA, 150 nmol/L of each primer, and 5 μL of SYBR Green PCR Master Mix (Applied Biosystems) in a total volume of 20 μL. For each biological sample, qPCR reactions were performed in triplicate on an Applied Biosystems Prism 7500HT Sequence Detection System. Individual receptor PCR efficiencies were calculated from the slope of the resulting standard curves, using the formula $E = 10^{-1/slope}$, where E is efficiency.[14,15]

Statistical Analysis

All results are expressed as mean ± SEM. Multiple groups were tested by 1-way analysis of variance followed by Holm's[22] procedure. Wilcoxon signed-rank was used to test differences between normal and tumor samples from the same patient or mouse. *P* values were adjusted for multiple comparisons according to Holm's[22] method. Changes in expression levels from normal mucosa to tumors (in FAP patients and $Apc^{Min/+}$ mice) and with or without APC-inducible expression in HT29 were first classified as positive or negative. Eventually, gene clustering to predict a positive or negative change was assessed via random forests.[23,24] With the random forest technique, 1000 trees were built to classify positive changes in APC status according to NRs in the APC-HT29 sample (n = 480, 10 experimental samples for 48 NRs). The training set used to grow each tree is a 0.632+ bootstrap resample of the observations.[25] Trees were allowed to grow to their full size without pruning, and nodes with at least 1 event and minimum total size of 5 were used as stopping rules. Furthermore, the best split at each node was selected from a 7-dimension random subset of the NRs (ie, the square root of the NRs). The out-of-bag observations then were classified to obtain the prediction error rate of the considered tree. The predictive ability of the classifier was assessed aggregating the single tree error rates, and a plot of the variable importance ranking obtained from the random forest was displayed. Finally, the same random forest was used to classify APC status in FAP patients (n = 480, 10 patient samples for 48 NRs) and $Apc^{Min/+}$ mice (n = 490, 10 mouse samples for 49 NRs) samples and the prediction error rates were assessed. *P* values less than .05 were considered significant. Data distribution and gene expression statistical analysis was performed using NCSS Statistical and Power Analysis Software 2007 (Kaysville, UT). For the random forest analysis we used the package randomForest version 4.5 (Salford Systems; San Diego, CA) implemented in R.

Results

NR Intestinal Localization Patterns

Because describing when and where genes are transcribed is a powerful method to elucidate their function,[14–16,26] we mapped the localization pattern of the entire NR family in the intestinal epithelium. To this end, we used previously validated high-resolution ISH[16] to label each receptor within the crypt-to-villus axis of the ileum and within the crypt to epithelium axis of the colon in C57BL/6 male mice. This analysis gave us the possibility to define for each receptor an expression pattern based on their transcript localization in the ileum and the colon (U, ubiquitous; C, crypt; V, villus; E, epithelium; or ND, not detectable in the epithelium; Figure 1). Furthermore, we also provided a semiquantitative estimate of NR messenger RNA (mRNA) abundance via independent scoring by different investigators (Supplementary Table 2). Although some NRs were not detected at a significant level in the epithelial cell type of both ileum and colon (*Ar*, *Dax*, *Fxrβ*, *Pnr*, *Pr*, *Rorα*, *Rorβ*, *Sf1*, *Shp*, *Tlx*, *Tr2*), the localization pattern of those NRs that were detected revealed a fascinating distribution along the crypt-villus/epithelium axis of the small and large intestine. Because we focused our analysis on the epithelium, the *ND* annotation does not exclude NR expression in the submucosal layers and/or endocrine, lymphoid, or mesenchymal cells (eg, *Rorα* in lymph nodes). This also can explain the apparent discrepancies between ISH and RTqPCR because the latter does not discriminate between specific cell types. Overall, between the ileum and the colon there is a high correspondence of epithelial localization pattern for the majority of the NRs. Interestingly, *Coup-TFI*, *Coup-TFII*, *Lrh1*, *Nurr1*, *Nor1*, *NfgIb*, *Pparβ/γ*, and *Trα* appear to be localized mostly between the proliferative progenitors cells and the lower third of the crypt. This suggested that these NRs, which are localized in the proliferative compartment of the intestinal crypt, eventually might play a role in the transcriptional regulation of proliferative-anabolic events. Another group of NRs (*Car*, *Errβ*, *Errγ*, *Lxrβ*, *Pparα*, *Rarα*, *Rxrβ*) is localized more ubiquitously in the intestinal mucosal epithelium. These NRs could play a role for the transcriptional regulation of proteins involved in both proliferative and differentiating epithelial cells. Finally, there is another group of NRs that are expressed mostly in the fully differentiated cells lining the intestinal epithelium of the ileum and colon. Within this last group of NRs, the sensors for bile acids (*Fxrα*), vitamin D (*Vdr*), glucocorticoids (*Gr*), xenobiotics (*Pxr*), mineralcorticoids (*Mr*), and estrogen-related compounds (*Errα*) are found. Illustrative examples of ISH typical for these respective expression patterns are shown in Figure 2, whereas the entire set of NRs is shown in Supplementary Figures 1 (ileum) and 2 (colon).

NR Intestinal mRNA Abundance in Normal Intestine and Tumors

After defining the intestinal localization pattern of the NR family, we compared the mRNA levels of each individual NR between normal intestinal epithelium and neoplastic intestinal tissue. We thus aimed to understand how the NR transcriptome is affected during the transition from normal to transformed epithelium. First, we used $Apc^{Min/+}$ mice,[21] which is a well-established mouse model to study CRC. Profiling the 49 mouse NRs by RTqPCR[14–18] in tumors and adjacent normal proximal colon epithelium enabled us to subdivide the entire NR family depending on their mRNA abundance pattern (Figure 3*A* and *B*). Although *Sf1* and *Tlx* were absent in both normal tissues and in tumors, a majority of the NRs were expressed robustly in normal (29 NRs) as well as in tumoral (26 NRs) intestine. The remaining NRs were

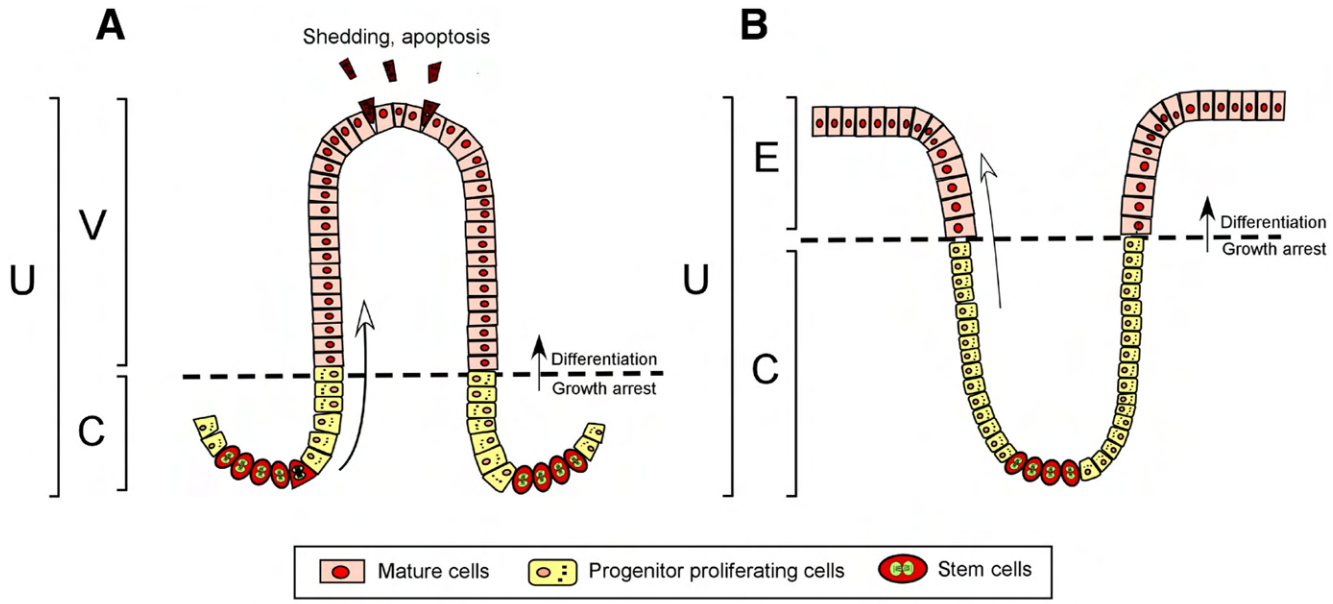

C

Localization patterns in the ileum

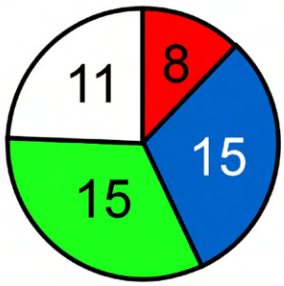

Crypts	Ubiquitous		Villus		N.D.	
COUP-TFI	CAR	RARα	EAR2	LXRα	AR	SF1
COUP-TFII	ERα	RARβ	ERβ	MR	DAX	SHP
LRH1	ERRβ	RARγ	ERRα	PXR	FXRβ	TLX
NURR1	ERRγ	RORγ	FXRα	REV-ERBα	PNR	TR2
NOR1	LXRβ	RXRβ	GR	REV-ERBβ	PR	
NGFIB	PPARα	RXRγ	HNF4α	RXRα	RORα	
PPARδ	PPARγ	TRβ	HNF4γ	TR4	RORβ	
TRα	GCNF1			VDR		

D

Localization patterns in the colon

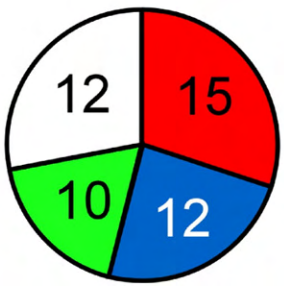

Crypts		Ubiquitous		Epithelium	N.D.	
COUP-TFI	RARγ	CAR	REV-ERBα	ERβ	AR	SF1
COUP-TFII	RORγ	ERα	REV-ERBβ	ERRα	DAX	SHP
EAR2	RXRβ	GCNF1	TR4	FXRα	ERRβ	TLX
LRH1	RXRγ	HNF4γ	ERRγ	GR	FXRβ	TR2
NGFIB	TRα	LXRβ		HNF4α	PNR	
NOR1	TRβ	PPARα		LXRα	PR	
NURR1		RARα		MR	RORα	
PPARδ		RARβ		PXR	RORβ	
PPARγ				VDR		
				RXRα		

Figure 1. Schematic representation of anatomic compartments in the intestinal epithelial axis and distribution of NR transcripts in mouse and human intestine. (*A*) Small intestine and (*B*) colon tissue anatomy. At the bottom of the crypt there are stem cells and progenitor proliferating cells. On the top of the villus in the ileum and surface epithelium in the colon there are mature differentiated enterocytes. We annotated the level of expression of NRs on the basis of their epithelial localization in the crypt (C), in the villus for the ileum (V), in the epithelial surface for the colon (E), or along the entire axis (U) as defined in the scheme. For the semiquantitative estimate of the ISH signal intensity see Supplementary Table 2. The scheme has been adapted and modified from Clevers,[1] D'Errico and Moschetta,[12] and Reya and Clevers.[43] NRs in normal (*C*) ileum and (*D*) colon were grouped into 4 categories based on their expression pattern and localization. NRs that are expressed in the crypts are in *red*, ubiquitously expressed NRs are in *blue*, NRs expressed in villus/epithelium are in *green*, and no detectable (N.D.) NRs are in *white*. The number of members of each group is indicated in pie charts and their names are listed in the corresponding tables.

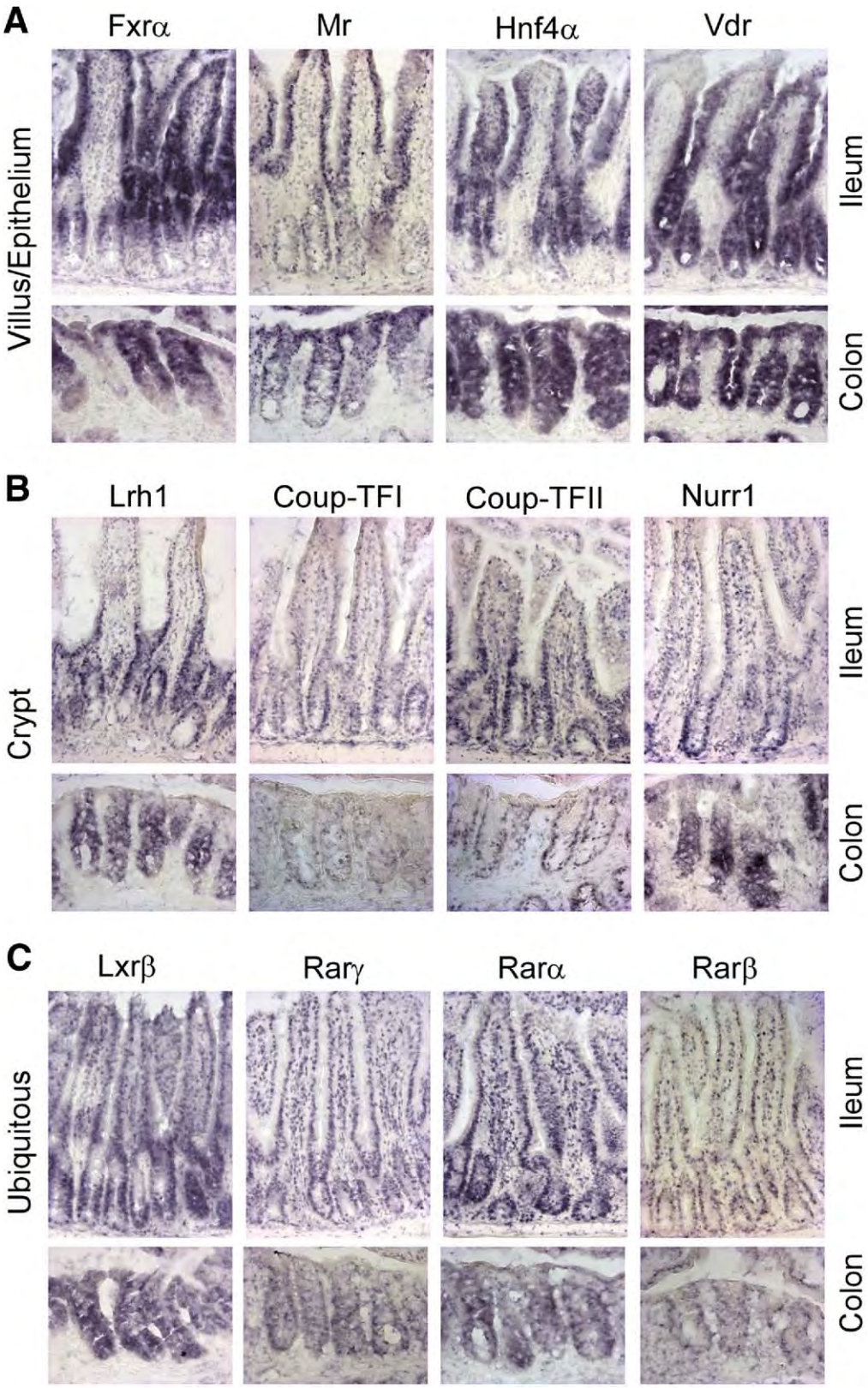

Figure 2. Localization pattern of NR in the intestinal epithelial axis. Examples of NR transcripts that are localized in (*A*) villus/epithelium, (*B*) crypt, or ubiquitously in (*C*) normal ileum and colon using nonradioactive ISH. The complete panel of localization pattern of NR transcripts is available in Supplementary Figures 1 and 2 for ileum and colon, respectively.

divided between those with low levels of expression (6 NRs in both normal tissues and tumors) and those that were expressed in moderate levels (12 NRs in normal tissues and 14 NRs in tumors). Comparing normal tissue with tumor tissue, the mRNA expression of most of the NRs was down-regulated (eg, *Car*, *Gr*, *Fxrα*, *Pparα* from high to moderate expression levels), whereas a more limited number of NRs were up-regulated (eg, *Erα* from

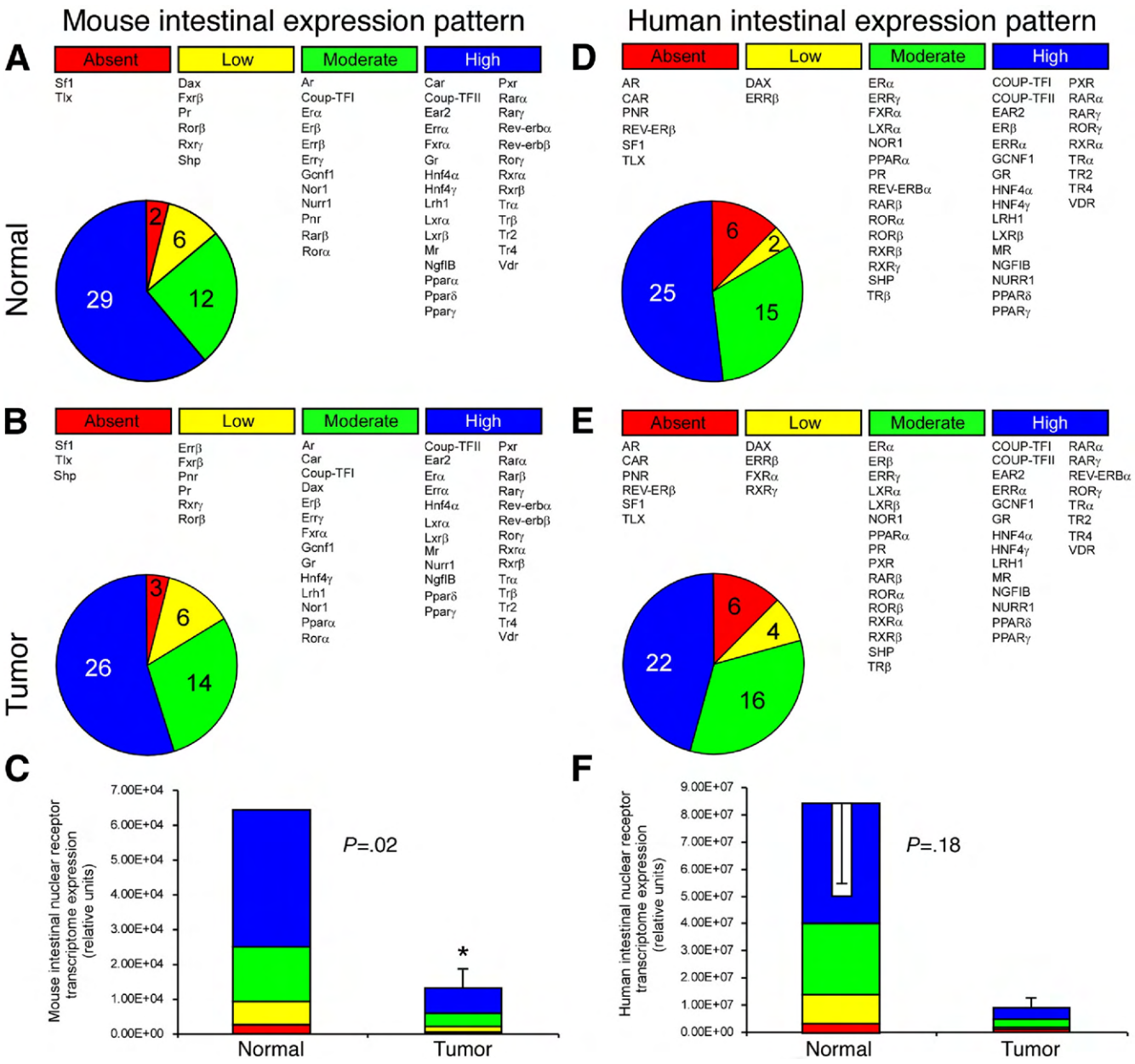

Figure 3. Expression levels of NRs in normal and tumor samples obtained in mice and human beings. NRs expressed in normal proximal colon (*A* and *D*, respectively) and adjacent tumor region (*B* and *E*, respectively) in human beings and mice were grouped into 4 categories based on their expression levels. Absent NRs are in *red*, low expressed NRs are in *yellow*, NRs with moderate expression levels are in *green*, and NRs with high expression levels are in *blue*. The number of members of each group is indicated in pie charts and their names are listed in the corresponding table. Summary of the entire NR transcriptome in normal proximal colon is compared with tumor samples in (*C*) mouse and (*F*) human beings. NR transcriptome levels are expressed as relative units and the fractions of the different groups of NRs are indicated by corresponding colors.

moderate to high expression levels) in tumor tissue. Interestingly, although expression levels changed, for a majority of NRs the mRNA expression patterns were unmodified. This leads us to conclude that overall the mouse intestinal NR transcriptome is strongly reduced in APC-initiated tumors (Figure 3*C*).

To evaluate whether our data in the $Apc^{Min/+}$ mouse model also were relevant to the human condition, we monitored the change of the NR transcriptome between normal and neoplastic tissues collected during colonoscopy from FAP patients[3] (Figure 3*D* and *E*). The presence of a germline and somatic mutation in the *APC* gene in the tumors was analyzed in the entire group of FAP patients. Profiling the 48 human NRs in normal tissues and tumors of FAP patients showed that apart from a few NRs, such as *androgen receptor*, *constitutive androstane receptor*, *photoreceptor-specific nuclear receptor*, and *REV-ERBβ*, which are expressed in the mouse but are absent in the human colon, the mRNA expression of the majority of the other NRs was comparable between the $Apc^{Min/+}$

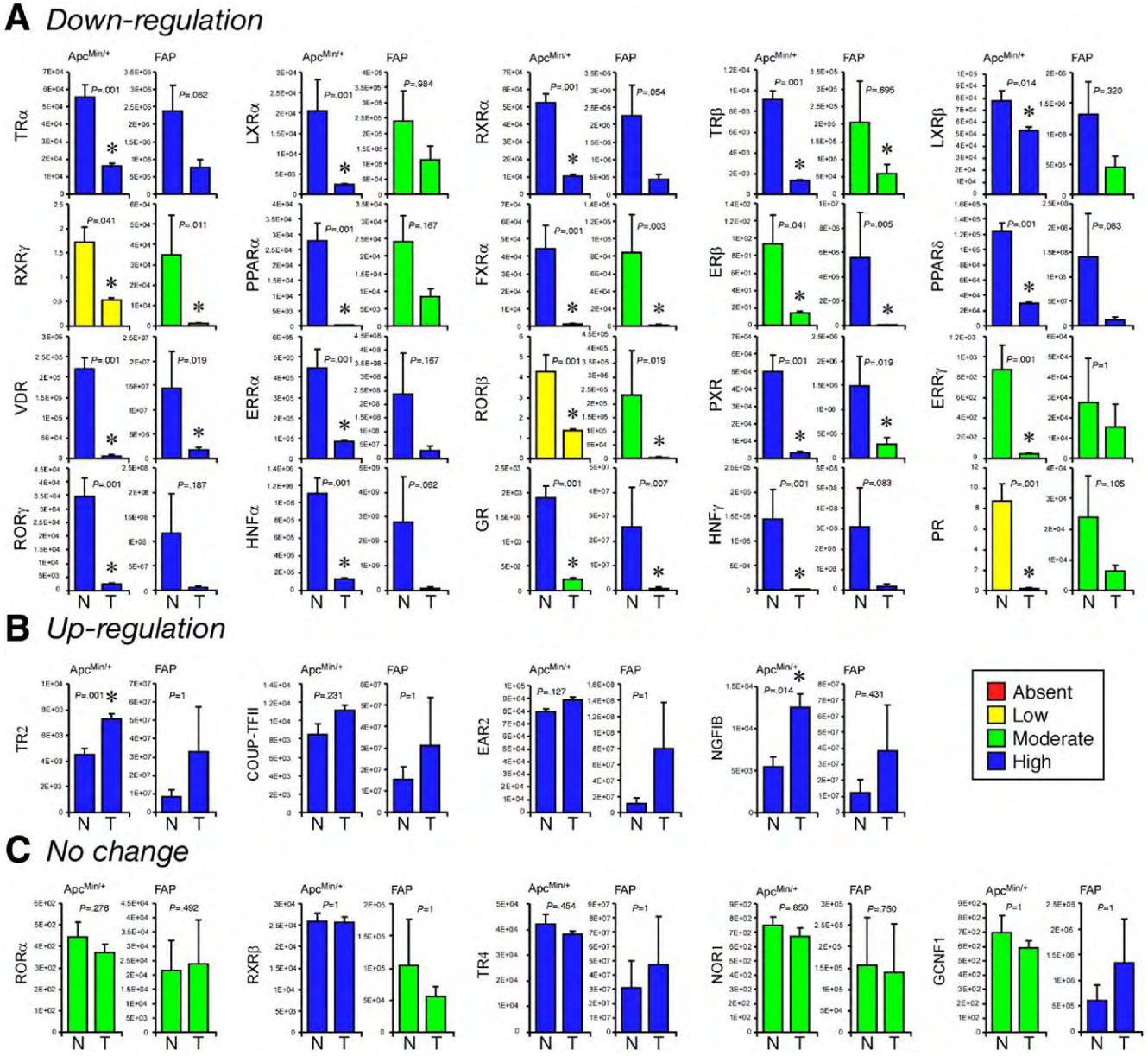

Figure 4. Expression modification of NRs in colon tumors in mice and human beings. Clustering members of the NR family, whose expression is (*A*) down-regulated, (*B*) up-regulated, and (*C*) unchanged in colon tumors of both mouse ($Apc^{Min/+}$) and human (FAP) models of CRC when compared with the adjacent normal intestinal epithelium. Genes are represented in 3 different colors based on their expression levels in normal and tumor samples (*yellow*, *green*, and *blue* for low, moderate, and high expression, respectively). Values are expressed as relative units and are plotted as the mean ± SEM of 12 mice and 10 patients. *P* values for significant differences are reported in Supplementary Table 3.

mouse and human FAP patients, underlining the translational relevance of our findings (Figure 3*D* and *E*). When comparing the overall mouse and human intestinal NR transcriptome between normal mucosa and tumors, there was a highly significant overall decrease in the mRNA expression levels for most NRs in the tumors (Figure 3*C* and *F*). These data hence unequivocally show an overall down-regulation of the NR transcriptome in both the murine and human model of CRC when progressing from normal intestinal epithelia to dysplastic lesions of the intestine.

After clustering the NRs on the basis of their expression levels, we wanted to quantify the changes in gene expression levels between normal and tumor samples for individual NRs. The entire picture of NR expression changes in $Apc^{Min/+}$ mice and FAP patients is reported in Supplementary Figures 3 and 4 and in Supplementary Table 3. In Figure 4 we have grouped those NRs that have similar expression patterns in $Apc^{Min/+}$ and FAP models when comparing normal and tumor tissues. No less then 20 NRs (close to half of the expressed NRs) were down-regulated in tumors in both models of CRC with respect

to adjacent tumor-free regions (Figure 4*A*). Strikingly, within this group of NRs are those NRs whose expression is maximal in the top of the epithelium of the colon, including *farnesoid X receptor-α*, *vitamin D receptor* (*VDR*), *pregnane X receptor*, *estrogen-related receptor-α*, *glucocorticoid receptor*, *liver X receptor-α*, and the orphan NR *hepatocyte nuclear factor-4α* (Figure 4*A*). The expression of another group of NRs was increased in both $Apc^{Min/+}$ and FAP models of CRC when comparing normal tissues with tumors (Figure 4*B*). These NRs include *TR2*, *chicken ovalbumin upstream promoter-transcription factor-II*, *EAR2*, and *neuronal growth factor 1B*, whose expression normally is restricted to the crypts of the colon. Finally, the expression of some NRs did not change between normal and tumor samples from $Apc^{Min/+}$ mice and FAP patients and those were mostly the NRs with an ubiquitous distribution pattern in the crypt-epithelium axis (Figure 4*C*).

NR Expression Levels in APC-Mutated Colon Cancer Cells With Inducible Wild-Type APC Protein

The APC gene is believed to be the gatekeeper in CRC development because mutations in this gene already are detectable in aberrant crypt foci and present in 85% of CRCs. However, tumor formation is a long process that requires many accumulated alterations in oncosuppressor genes as well as in oncogenes that also could influence or be influenced by changes in NR expression. In the effort to define those NRs whose modified expression in APC-initiated tumors depends on the presence of an APC mutated protein, we compared the mRNA levels of the NR family in human CRC cells harboring an APC-mutated protein (together with several other mutations) with their expression after re-induction of a wild-type APC protein by 24-hour treatment with $ZnCl_2$[20] (Figure 5*A* and *B*). In this cell system, the majority (30 of 48 total) of the NRs already was robustly expressed before re-expression of wild-type APC. Eleven NRs were considered absent before $ZnCl_2$ treatment, whereas only 5 NRs remained absent after $ZnCl_2$ induction of the wild-type APC protein. Furthermore, NRs such as *constitutive androstane receptor*, *glucocorticoid receptor*, *photoreceptor-specific nuclear receptor*, *progesterone receptor*, *retinoic acid receptor–related orphan receptor-β*, and *retinoid X receptor γ* (*RXRγ*), which were not expressed before, become expressed after $ZnCl_2$. The rest of the NRs could be divided into those with low expression (7 NRs before $ZnCl_2$ treatment and 9 NRs after $ZnCl_2$ treatment) and those with moderate levels of expression (7 NRs before $ZnCl_2$ treatment and 11 NRs after $ZnCl_2$ treatment). Although differences were evident in individual members of the family, the overall NR transcriptome expression was unchanged after restoring expression of the wild-type APC protein (Figure 5*C*). We also quantified the changes in gene expression levels for individual NRs before and after re-expression of wild-type APC protein (the entire set of data is available in Supplementary Figure 5 and in Supplementary Table 3). The expression of some NRs whose levels are reduced in tumors is induced by restoring the wild-type APC protein in HT29 cells (Figure 5*D*). This is the case for *thyroid receptor-β*, *peroxisome proliferator-activated receptor-γ*, *retinoic acid receptor–related orphan receptor-β*, *farnesoid X receptor-α*, *VDR*, *pregnane X receptor*, *RXRγ*, *estrogen receptor-β*, *glucocorticoid receptor*, and *progesterone receptor*, highlighting the dependence of these NRs on the APC pathway in both mouse and human models of CRC. Conversely, the expression of NRs whose transcript is induced in tumors is down-regulated when restoring a wild-type APC in HT29 cells, as illustrated for *chicken ovalbumin upstream promoter-transcription factor-II* and *EAR2* (Figure 5*E*). Finally, we found 3 NRs, *retinoic acid receptor–related orphan receptor-α*, *RXRβ*, *TR4*, whose expression was not affected in tumors, as well as after re-expression of a wild-type APC protein (Figure 5*F*). Overall, the canonical Wnt-APC pathway seems to be one of the main regulators of NR localization in the intestine and of their expression in tumors.

Comprehensive Overview and Classification Trees

This entire set of data positioned us well to provide a final comprehensive overview of the coordinate regulation of NR expression in relation to the development of CRC. First, we present in Figure 6*A* an easy-go-through chart summarizing the expression patterns of the entire NR family and their modification during tumorigenesis in the 3 APC-initiated tumor models studied. Second, we distilled a statistical method that predicts the modification of NR expression in tumors based on their expression localization along the intestinal crypt-villus axis (Figure 6*B*). NRs that were localized specifically in the lower third of the crypt in the colon were induced in tumors. On the contrary, the expression of NRs localized in the differentiated epithelium was decreased in tumors. Those NRs that were expressed ubiquitously in the crypt-to-epithelial axis served as an important control because their expression was not modified significantly during neoplastic transformation. We then classified NRs into 2 distinct groups based on their decreased or increased expression in tumor samples. We used the mRNA abundance in human HT29-APC inducible cells to subdivide the clusters and to study the prediction of NR expression modification in the human and mouse normal intestine and tumor samples. Our analysis revealed the power to predict the class to which a given NR belongs. Indeed, using random forests classification, prediction error rates for the HT29-APCi cells, FAP patients, and $Apc^{Min/+}$ mice were 10.2%, 48.5%, and 43.1%, respectively. Supplementary Figure 6 shows the variable importance ranking obtained from the random forest classification in the HT29-APC sample.

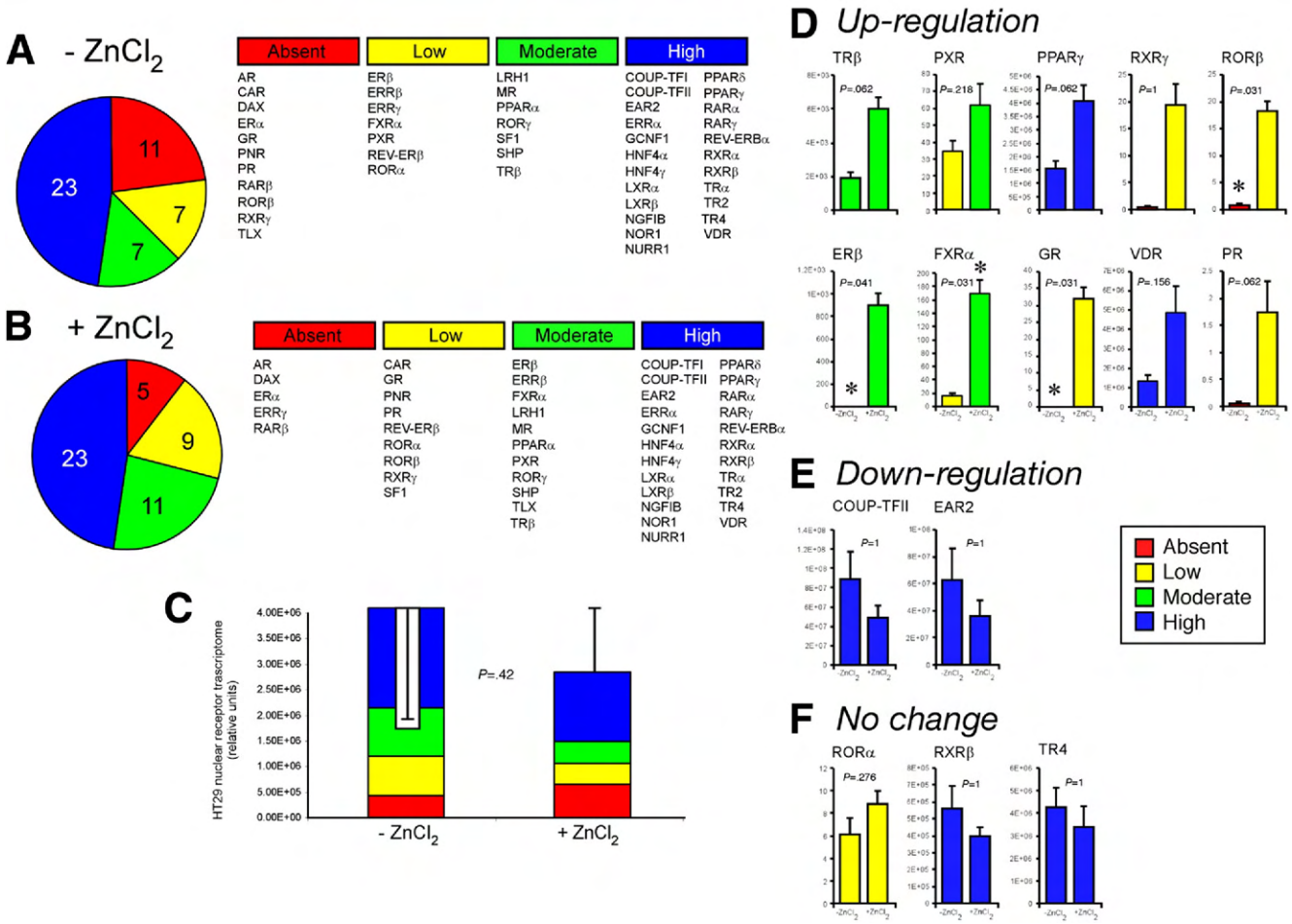

Figure 5. NR expression profile in HT29 cells in which the expression of wild-type APC was re-induced. NRs in HT29-APC–inducible cells (*A*) before and (B) after restoration of the expression of wild-type APC protein by $ZnCl_2$ treatment were grouped into 4 categories based on their expression levels: absent in *red*, low in *yellow*, moderate in *green*, and high in *blue*. The number of the members of each group is indicated in the pie charts and their names are listed in the corresponding tables. (*C*) NR transcriptome in HT29-APC–inducible cells before and after restoration of wild-type APC protein via $ZnCl_2$ are compared and expressed as relative units. The fractions of the different groups of NR are indicated by corresponding colors. (*D–F*) mRNA expression levels of NRs in HT29-APC–inducible cells without and with treatment with $ZnCl_2$ (ie, with and without re-expression of a wild-type APC protein that is mutated in colon cancer HT29 cells). (*D*) NRs that are up-regulated in HT29-APC–inducible cells after restoration of wild-type APC protein represent the same group of NRs that are down-regulated in colon tumors relative to the adjacent normal region of both mouse ($Apc^{Min/+}$) and human (FAP) models of CRC. (*E*) NRs that are down-regulated in HT29-APC–inducible cells after restoration of wild-type APC protein represent the same group of NRs that are up-regulated in colon tumors with respect to the adjacent normal region of both mouse ($Apc^{Min/+}$) and human (FAP) models of CRC. (*F*) NRs that do not change in HT29-APC–inducible cells after restoration of wild-type APC protein represent the same group of NRs that also do not change in colon tumors with respect to the adjacent normal region of both mouse ($Apc^{Min/+}$) and human (FAP) models of CRC. Genes are represented in 4 different colors based on their expression levels in cells treated and not treated with $ZnCl_2$ (*red*, *yellow*, *green*, and *blue* for absent, low, moderate, and high expression, respectively). Values are expressed as relative units and plotted as the mean ± SEM of 6 experiments in triplicate. *P* values for significant differences are reported in Supplementary Table 3.

We finally aimed to validate the data obtained in mRNA abundance in terms of protein expression. We were able to validate few antibodies against NRs that allowed us to perform immunohistochemical analysis in the normal colon mucosa and in tumors. We choose NRs with different localization and expression patterns (ie, predominately expressed in the crypt or in the epithelium or ubiquitously) (Supplementary Table 2, Fxr*α*, Vdr, Rxr*β*, Nor1, Ear2). We also used antibodies against Ki67 and L-Fabp as markers of the proliferative and differentiated compartments of the intestinal mucosal crypt-to-epithelium axis, respectively. We then labeled proximal and distal colon, rectum, and tumors from the same mice to also validate our expression modification profile pattern (Figure 7). For the proteins that we examined, we were able to almost completely reproduce the mRNA and ISH data because Fxr*α* was expressed abundantly in the upper epithelium region and was decreased in tumors; Vdr was expressed ubiquitously, although more in the epithelium, and decreased in tumors; Rxr*β* and Nor1 were expressed in crypts and their expression was unchanged in tumors; Ear2 showed major expression levels

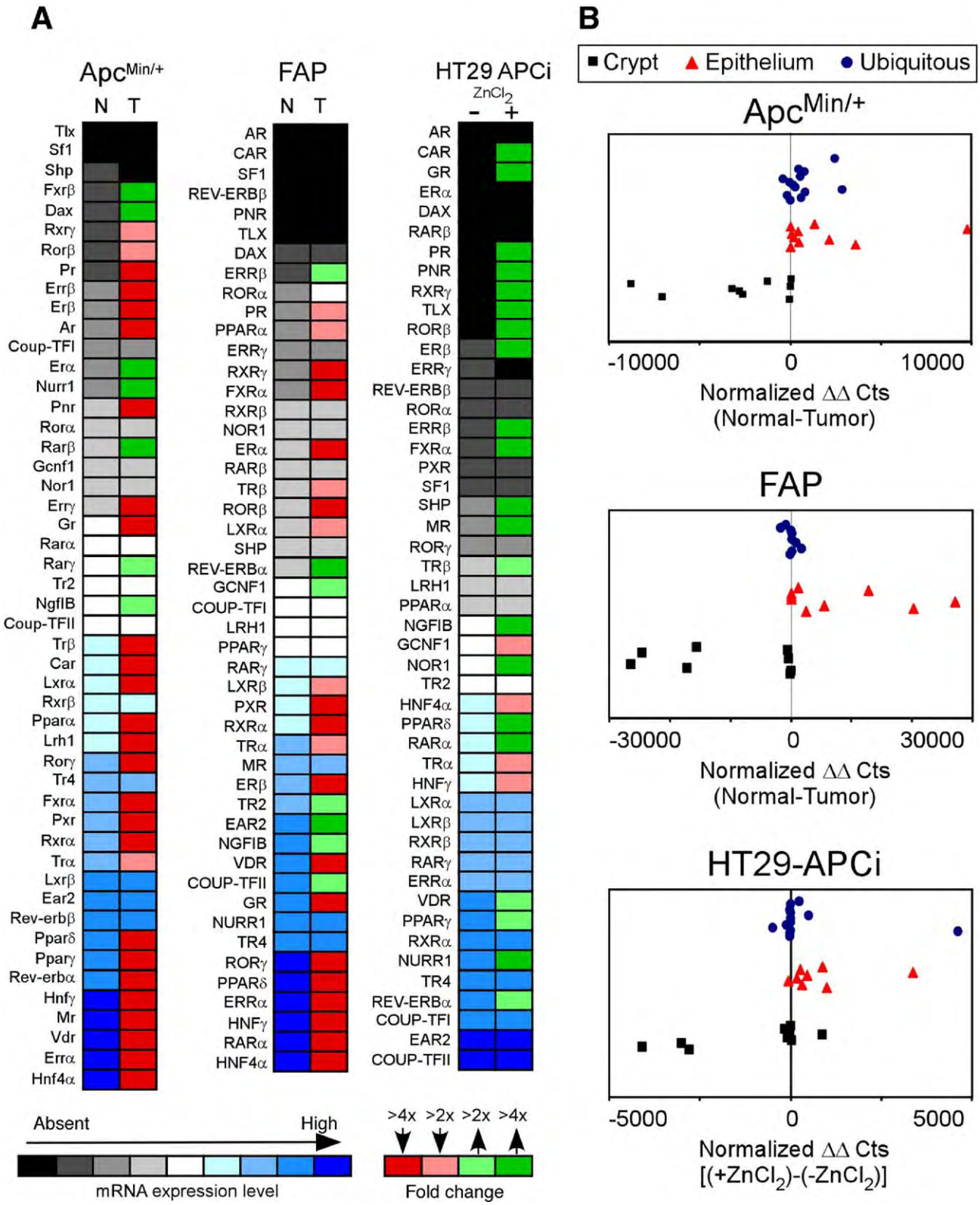

Figure 6. NR expression modulation chart in the 3 different models of APC-initiated tumors and prediction models for intestinal NR localization and expression modulation in tumors. (*A*) Schematic representation of the entire NR transcriptome by RTqPCR with different colors representing different mRNA expression levels and fold change in expression levels between normal and tumor samples in $Apc^{Min/+}$ mice and FAP patients and between $ZnCl_2$-untreated and $ZnCl_2$-treated HT29 cells. (*B*) Intestinal cell localization predicts expression modulation in tumors. In the 3 models of APC-initiated tumor study, NRs that were localized specifically in the lower third of the crypt in the colon were induced significantly in tumors. On the contrary, NRs localized in the differentiated epithelium were down-regulated significantly in tumors. Those NRs that were expressed ubiquitously in the crypt-to-epithelial axis served as a significant control because their expression was not modified significantly during neoplastic transformation.

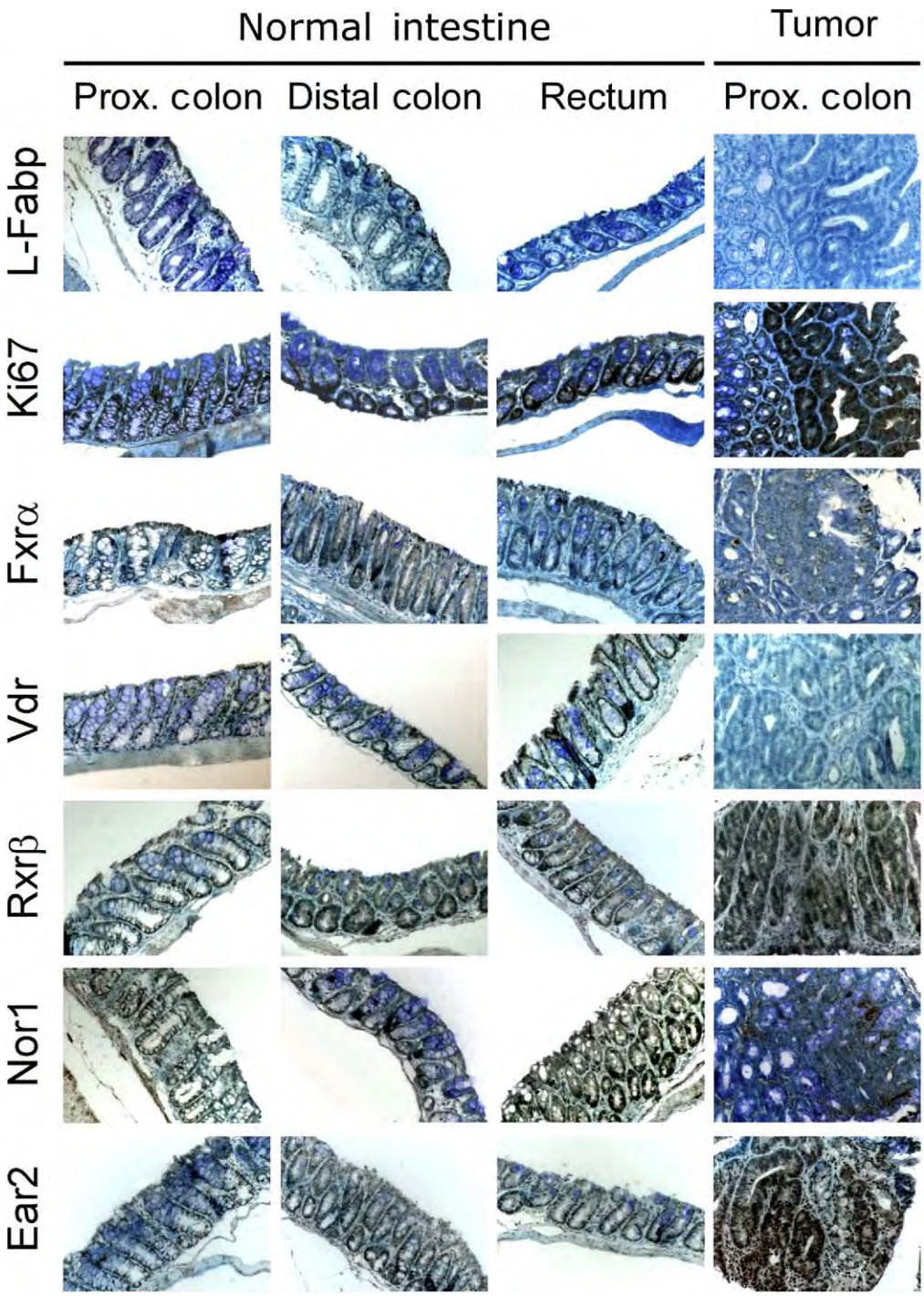

Figure 7. NR protein expression in normal intestine and tumors. Expression levels and localization of L-Fabp, Ki67, and the NRs Fxrα, Vdr, Rxrβ, Nor1, and Ear2 in mouse normal intestine and tumors. Paraffin-embedded proximal colon, distal colon, and rectum specimens were immunostained with antibodies against Fxrα, Vdr, Rxrβ, Nor1, and Ear2 proteins to determine their expression and localization. Immunostaining of L-Fabp and Ki67 was used as markers of the differentiated mucosal cells of the epithelium and the proliferative crypt compartment of the crypts, respectively (magnification, 200×).

in the proliferative compartment with further increased levels in tumors with respect to normal mucosa. Also for the NRs studied, no significant difference in the pattern of localization in the intestinal epithelium has been detected between proximal and distal colon and rectum.

Discussion

The characterization of the NR transcriptome in the normal intestine and tumors constitutes an important resource, which opens up new roads to investigate the roles of individual or groups of NRs in the pathogenesis and progression of CRC.[4–6] Importantly, clustering NRs on the basis of their different localization into the crypt-villus axis of the normal intestine sheds light on their function. In fact, the activity of NRs that are highly expressed in the proliferative progenitors cells of the lower crypt unit are related to energy demand, cell division, and cell-cycle promitotic pathways. Also, their levels of expression as well as their activities seem directly interdependent on the activity of the *Wnt* signaling.[12,13]

The power of our analysis is based on the capacity to monitor the relationship between localization and modulation of the expression of NR clusters during the passage from proliferative progenitors to differentiated enterocytes, as well as from a normal intestinal epithelium to an APC-initiated tumor tissue. Intriguingly, the localization map of these proteins within the crypt-villus axis predicts their expression modulation in tumors. In fact, NRs whose mRNA expression is restricted mostly in the lower third of the colonic crypt were highly expressed in tumors. On the other hand, a set of NRs, which is expressed during intestinal cell migration and differentiation, is almost completely absent in tumor tissue. Confirming the validity of this hypothesis, re-expressing wild-type APC protein in CRC cells with APC mutation re-induces the NR cluster that normally is present in the intestinal epithelium differentiated cells.

Several transgenic animal models for NR gain and loss function[12,13] have been generated in the recent past to study the role of some of these proteins in intestinal tumorigenesis. Intriguingly, we were able to validate our present findings for some of the published discoveries in mouse models. For NRs that are localized in the proliferative compartment of the intestinal crypts, such as liver receptor homolog-1, a clear role in promoting the promitotic activity through the transcriptional regulation of genes such as cyclin E1 has been shown.[27] Moreover, liver receptor homolog-1 haploinsufficiency in mice decreases intestinal tumorigenesis in chemical and genetic mouse models of cancer,[28] with a net decreased ability of mice to regenerate their intestinal mucosa.[29] On the other hand, NRs that are localized in the differentiated compartment of the intestinal epithelium, such as VDR, estrogen receptor-β, and farnesoid X receptor-α, have been shown to play an antitumoral role in mice.[30,31] Indeed, loss of VDR and estrogen receptor-β in mice results in colon cell hyperproliferation and increased susceptibility to tumor formation.[30–32] Interestingly, activation of both VDR and estrogen receptor-β in xenograft, chemical, and genetic models of intestinal tumors results in a strong decrease in total tumor load and cell growth,[30,31,33,34] thus highlighting the putative therapeutic potential of targeting NRs in colon cancer. Moreover, NRs whose activity has been shown to modulate both proliferative and apoptotic pathways in the intestine such as peroxisome proliferator-activated receptor-γ[35–38] and RXRs-retinoic acid receptors[39,40] maintain a sustained expression abundance in tumors, and thus could be of potential pharmacologic importance in colon cancer.

In the present study we characterized APC-initiated intestinal precancerous lesions from human subjects with FAP and mice in which intestinal tumorigenesis was initiated by the same genetic mutation.[3] Unraveling the expression changes of NRs in this early initial step of CRC is important if one recognizes the relevance of this family of transcription factors in the regulation of cellular pathways driven by steroid hormones and lipids of dietary and endogenous origins.[7] In fact, dietary and hormonal stimuli are among the main epidemiologically recognized determinants that control the timing of the multistep process of CRC.[41,42] Our data, therefore, not only provide an unparalleled tool for the scientific community, but also could have a great translational value. The presence of specific ligand binding domains in most members of the NR family has pointed to design or to identify specific chemicals able to activate or inhibit the transcriptional activity of these proteins.[11] Indeed, the NR family represents an attractive group of proteins in that novel drugs could target them. Synthetic or natural compounds able to modify NR activity are used commonly to prevent and treat several diseases such as diabetes, dyslipidemia, metabolic syndrome, and various types of cancer, including solid and nonsolid tumors.[11] Thus, those NRs known to regulate cell differentiation and/or apoptosis that in tumors, even if down-regulated, retain a high to moderate expression could be targeted with agonists for the management of CRC. On the other hand, NRs that are expressed in the intestinal crypts, up-regulated in tumor tissues, and are involved directly in proliferation processes could be used as novel diagnostic markers for early stage tumors and eventually targeted with antagonists if their functional activation is constitutively necessary for the metabolic requirements of a tumoral cell. Overall, our unique and comprehensive NR expression atlas in CRC may provide an impetus to characterize their role further in CRC pathogenesis and perhaps one day supply a more successful therapy ad personam.

Supplementary Materials

Note: To access the supplementary material accompanying this article, visit the online version of *Gastroenterology* at www.gastrojournal.org, and at doi: 10.1053/j.gastro.2009.09.060.

References

1. Clevers H. Wnt/beta-catenin signaling in development and disease. Cell 2006;127:469–480.
2. van de Wetering M, Sancho E, Verweij C, et al. The beta-catenin/TCF-4 complex imposes a crypt progenitor phenotype on colorectal cancer cells. Cell 2002;111:241–250.
3. Kinzler KW, Nilbert MC, Su LK, et al. Identification of FAP locus genes from chromosome 5q21. Science 1991;253:661–665.
4. Fearon ER, Vogelstein B. A genetic model for colorectal tumorigenesis. Cell 1990;61:759–767.
5. Vogelstein B, Kinzler KW. Cancer genes and the pathways they control. Nat Med 2004;10:789–799.
6. Kinzler KW, Vogelstein B. Lessons from hereditary colorectal cancer. Cell 1996;87:159–170.
7. Mangelsdorf DJ, Thummel C, Beato M, et al. The nuclear receptor superfamily: the second decade. Cell 1995;83:835–839.
8. Mangelsdorf DJ, Evans RM. The RXR heterodimers and orphan receptors. Cell 1995;83:841–850.
9. Francis GA, Fayard E, Picard F, et al. Nuclear receptors and the control of metabolism. Annu Rev Physiol 2003;65:261–311.

10. McKenna NJ, O'Malley BW. Combinatorial control of gene expression by nuclear receptors and coregulators. Cell 2002;108:465–474.
11. Chawla A, Repa JJ, Evans RM, et al. Nuclear receptors and lipid physiology: opening the X-files. Science 2001;294:1866–1870.
12. D'Errico I, Moschetta A. Nuclear receptors, intestinal architecture and colon cancer: an intriguing link. Cell Mol Life Sci 2008;65:1523–1543.
13. Mulholland DJ, Dedhar S, Coetzee GA, et al. Interaction of nuclear receptors with the Wnt/beta-catenin/Tcf signaling axis: Wnt you like to know? Endocr Rev 2005;26:898–915.
14. Bookout AL, Jeong Y, Downes M, et al. Anatomical profiling of nuclear receptor expression reveals a hierarchical transcriptional network. Cell 2006;126:789–799.
15. Yang X, Downes M, Yu RT, et al. Nuclear receptor expression links the circadian clock to metabolism. Cell 2006;126:801–810.
16. Gofflot F, Chartoire N, Vasseur L, et al. Systematic gene expression mapping clusters nuclear receptors according to their function in the brain. Cell 2007;131:405–418.
17. Chuang JC, Cha JY, Garmey JC, et al. Nuclear hormone receptor expression in the endocrine pancreas. Mol Endocrinol 2008;22:2353–2363.
18. Fu M, Sun T, Bookout AL, et al. A nuclear receptor atlas: 3T3-L1 adipogenesis. Mol Endocrinol 2005;19:2437–2450.
19. Margolis RN, Evans RM, O'Malley BW. The nuclear receptor signaling atlas: development of a functional atlas of nuclear receptors. Mol Endocrinol 2005;19:2433–2436.
20. Morin PJ, Vogelstein B, Kinzler KW. Apoptosis and APC in colorectal tumorigenesis. Proc Natl Acad Sci U S A 1996;93:7950–7954.
21. Su LK, Kinzler KW, Vogelstein B, et al. Multiple intestinal neoplasia caused by a mutation in the murine homolog of the *APC* gene. Science 1992;256:668–670.
22. Holm S. A Simple Sequentially Rejective Bonferroni Test Procedure. Scand J Stat 1979;6:65–70.
23. Liaw A, Wiener M. Classification and regression by random forest. R News 2002;2:18–22. Available from: http://CRAN.R-project.org/doc/Rnews/.
24. Breiman L. Random forests. Machine Learning 2001;45:5–32.
25. Efron B, Tibshirani RJ. Improvements on cross-validation: the .632+ bootstrap method. J Am Stat Association 1997;92:548–560.
26. Zhang W, Morris QD, Chang R, et al. The functional landscape of mouse gene expression. J Biol 2004;3:21.
27. Botrugno OA, Fayard E, Annicotte JS, et al. Synergy between LRH-1 and beta-catenin induces G1 cyclin-mediated cell proliferation. Mol Cell 2004;15:499–509.
28. Schoonjans K, Dubuquoy L, Mebis J, et al. Liver receptor homolog 1 contributes to intestinal tumor formation through effects on cell cycle and inflammation. Proc Natl Acad Sci U S A 2005;102:2058–2062.
29. Coste A, Dubuquoy L, Barnouin R, et al. LRH-1-mediated glucocorticoid synthesis in enterocytes protects against inflammatory bowel disease. Proc Natl Acad Sci U S A 2007;104:13098–13103.
30. Wada-Hiraike O, Imamov O, Hiraike H, et al. Role of estrogen receptor beta in colonic epithelium. Proc Natl Acad Sci U S A 2006;103:2959–2964.
31. Modica S, Murzilli S, Salvatore L, et al. Nuclear bile acid receptor FXR protects against intestinal tumorigenesis. Cancer Res 2008;68:9589–9594.
32. Kallay E, Pietschmann P, Toyokuni S, et al. Characterization of a vitamin D receptor knockout mouse as a model of colorectal hyperproliferation and DNA damage. Carcinogenesis 2001;22:1429–1435.
33. Huerta S, Irwin RW, Heber D, et al. 1alpha,25-(OH)(2)-D(3) and its synthetic analogue decrease tumor load in the Apc(min) mouse. Cancer Res 2002;62:741–746.
34. Palmer HG, Gonzalez-Sancho JM, Espada J, et al. Vitamin D(3) promotes the differentiation of colon carcinoma cells by the induction of E-cadherin and the inhibition of beta-catenin signaling. J Cell Biol 2001;154:369–387.
35. Saez E, Tontonoz P, Nelson MC, et al. Activators of the nuclear receptor PPARgamma enhance colon polyp formation. Nat Med 1998;4:1058–1061.
36. Sarraf P, Mueller E, Jones D, et al. Differentiation and reversal of malignant changes in colon cancer through PPARgamma. Nat Med 1998;4:1046–1052.
37. Lefebvre AM, Chen I, Desreumaux P, et al. Activation of the peroxisome proliferator-activated receptor gamma promotes the development of colon tumors in C57BL/6J-APCMin/+ mice. Nat Med 1998;4:1053–1057.
38. Desvergne B, Wahli W. Peroxisome proliferator-activated receptors: nuclear control of metabolism. Endocr Rev 1999;20:649–688.
39. Yamazaki K, Shimizu M, Okuno M, et al. Synergistic effects of RXR{alpha} and PPAR{gamma} ligands to inhibit growth in human colon cancer cells phosphorylated RXR{alpha} is a critical target for colon cancer management. Gut 2007;56:1557–1563.
40. Xiao JH, Ghosn C, Hinchman C, et al. Adenomatous polyposis coli (APC)-independent regulation of beta-catenin degradation via a retinoid X receptor-mediated pathway. J Biol Chem 2003;278:29954–29962.
41. Faivre J, Boutron MC, Quiport V. Diet and large bowel cancer. In: Zappia V, ed. Advances in nutrition and cancer. New York: Plenum Press, 1993:107–108.
42. Lipkin M, Reddy B, Newmark H, et al. Dietary factors in human colorectal cancer. Annu Rev Nutr 1999;19:545–586.
43. Reya T, Clevers H. Wnt signalling in stem cells and cancer. Nature 2005;434:843–850.

Received January 21, 2009. Accepted September 29, 2009.

Reprint requests

Address requests for reprints to: Dr Antonio Moschetta, University of Bari, Consorzio Mario Negri Sud, Via Nazionale 8/A, 66030 Santa Maria Imbaro, Chieti, Italy. e-mail: moschetta@negrisud.it; fax: (39) 0872-570299.

Acknowledgments

The authors thank Drs K. W. Kinzler and B. Vogelstein for their precious tools. Scientific discussions on this topic with Drs H. Clevers and D. J. Mangelsdorf are gratefully acknowledged. The authors thank E. Bellafante, N. Chartoire, I. D'Errico, L. Evans, G. Lo Sasso, A. Morgano, M. Petruzzelli, and C. Simone for technical assistance and criticisms.

S.M. and F.G. equally contributed to this work.

Conflicts of interest

The authors disclose no conflicts.

Funding

This work was funded by the Italian Association for Cancer Research (Start-Up grant 2005, AIRC, Milan, Italy), University of Bari (ORBA07X7Q1 and ORBA06BXVC, Bari, Italy), CARISPAQ (L'Aquila, Italy), ERC-STG-FIRB-IDEAS (RBID08C9N7), INSERM, CNRS, Université Louis Pasteur (Strasbourg, France), and EPFL (Lausanne, Switzerland).

Supplementary Materials and Methods

ISH analysis was performed on both distal ileum and proximal colon; mRNA analysis in normal mucosa of $Apc^{Min/+}$ mice was performed in proximal colon; tumor analysis of $Apc^{Min/+}$ mice was performed on adenomas of the proximal colon; human tissues were obtained during endoscopy for tumors of the ascendant and transversus colon; and normal samples were obtained with biopsies of endoscopic apparent normal adjacent mucosa.

The Institutional Animal Care of the Consorzio Mario Negri Sud approved all animal experiments.

FAP Patients

In the present study we enrolled 10 patients with a clinical diagnosis of FAP, with histomorphologic confirmation of colonic adenomas and with a characterized germline mutation in the *APC* gene. The coding region of the *APC* gene, including all splice junctions, was amplified in a total of 28 fragments.[1] Exons 1–14 were amplified using primers located within intronic regions, whereas exon 15 was amplified as 14 overlapping fragments. Each amplified fragment was analyzed by denaturing high-performance liquid chromatography (Wave 1100; Transgenomic, Inc, Omaha, NE).[1,2] Samples that showed altered denaturing high-performance liquid chromatography profiles were sequenced directly using an ABI PRISMTM310 genetic analyzer (Applied Biosystems, Foster City, CA). Two APC mutations were diagnosed among the entire patient group (c.2527_2530 AGTT p.Ser843fsX860 and c.3927_3931 AAAGA p.Glu1309fsX1312), and no relevant differences for the present expression profiling study could be detected on the basis of this germline characteristic. Genomic DNA was isolated from at least 2 independently drawn whole-blood samples using QIAamp DNA Blood (Qiagen, Inc, Chatsworth, CA).

Cell Lines

Stable transfected APC-inducible HT29 cells were obtained from Drs K.W. Kinzler and B. Vogelstein and were cultured as previously described.[3] Cells were maintained in McCoy's 5A growth medium, supplemented with 10% fetal bovine serum and 0.6 mg/mL hygromycin B. Expression of wild-type APC protein was induced with (110 mmol/L) ZnCl2 for 24 hours in HT29 CRC cells containing the APC gene under the control of a modified metallothionein promoter. A cell line with an inducible *lacZ* gene (HT29-β-gal) was used as control.

Nonradioactive High-Resolution ISH

Particular attention has been paid during all processes, from the ordering of mice to the final annotation of ISH signal, to obtain rigorously validated data.

Samples collection and sectioning. During dissection, 4 segments were collected along the intestine (duodenum, jejunum, ileum, and colon) and embedded together side by side in the same block. During sectioning, the 4 segments thus were sectioned together. In addition, adjacent sections were partitioned on serial slides to have several sets of comparable slides be hybridized with different probes. This procedure allows each part of the intestine to be an internal control for the other parts during hybridization and increases the robustness of signal comparison between ileum and colon. The serial sections allow hybridizing of several genes on adjacent sections of the same intestine, and thus increase the robustness of signal comparison between different NRs.

Hybridization. To avoid the impact of slight variations between different hybridizations on the comparison between NR expression, we put a particular effort to hybridize all probes for all NRs in the same experiment. By this procedure, all probes are also used as a positive or a negative control for the others. For example, photoreceptor-specific nuclear receptor (PNR), which is expressed only in the retina, could act as a negative control, while Fxrα, which is particularly highly expressed in the intestine, could act as a positive control. Within each run, an additional negative control was used as one slide was hybridized with a sense probe for FXRα. Most importantly, all the probes used in this study have been validated previously on other tissues, mainly on the brain (see data at http://www-mci.ustrasbg.fr/mousepat/ and Gofflot et al[4]).

Data analysis. ISH experiments have been reproduced on a minimum of 3 different intestines (from 3 different mice) for each gene, and the results presented are a summary of the analysis of all hybridizations. In addition, as stated in the article, 3 independent observers scored the signal. Finally, the significance of the negative and positive results also was evaluated by comparison with expression data available on the Nuclear Receptor Signaling Atlas (NURSA) web site (see data at http://www.nursa.org/). These data have been obtained using RT-qPCR on intestine collected from C57BL/6 mice. All the genes that gave negative results in our hybridization were not detected at significant levels in the NURSA dataset, thus strengthening the validity of our results.

Immunohistochemistry

Tissue specimens were fixed in 10% formalin (pH 7.4) for 12–24 hours (Sigma-Aldrich, St. Louis, MO), dehydrated, and paraffin embedded. Standard immunohistochemical procedures were performed. Briefly, 5-μm–thick sections were treated with 3% hydrogen peroxide for 5 minutes to reduce endogenous peroxidase activity, and then subjected to antigen retrieval by boiling the slides in Antigen Unmasking Solution (Vector Laboratories, Inc, Burlingame, CA) for 10 minutes according to the manufacturer's instructions. Sections then were incubated in 50% nonimmune serum (from the host animal in which the secondary antibody was raised) in phosphate-buffered saline (PBS) for 30 minutes at room tem-

perature (to avoid aspecific signal) and incubated overnight at 4°C with the primary antibodies (rabbit polyclonal Ki67, FABP, and EAR2 [NR2F6] antibody, and rat polyclonal VDR from AbCam [Cambridge, MA], rabbit polyclonal antibody to RARα from Santa Cruz Biotechnology Inc [Santa Cruz, CA], rabbit polyclonal antibody to RXR-β from Upstate [Lake Placid, NY], rabbit polyclonal to NR NOR-1; Imgenex, San Diego CA). The following day, after 30 minutes at room temperature, sections were washed for 10 minutes in PBS 0.1 mol/L, and incubated for 30 minutes at room temperature with the secondary biotinylated antibody (Vector Laboratories); for anti-VDR a secondary anti-rat biotinylated antibody from AbCam was used. Sections then were washed carefully with PBS (3 washes, 5 min/each) and incubated with the avidin-biotin complex (Vector Laboratories) for 30 minutes at room temperature. After washing in PBS, the reaction of peroxidase was developed by the incubation of samples with 3,3′-diaminobenzidine tetrahydrochloride (Sigma-Aldrich). Counterstaining was performed with methylene-blue (Sigma-Aldrich). For negative controls, 1% nonimmune serum in PBS replaced the primary antibodies.

RNA Preparation and RTqPCR Analysis

RNA was extracted from tissues and cells using TRIzol Reagent (Invitrogen, Carlsbad, CA). RTqPCR primers were designed using Primer Express Software (Applied Biosystems). Human and mouse NR primer sequences are available on request. RTqPCR reactions contained 60 ng of complementary DNA, 150 nmol/L of each primer, and 5 μL of SYBR Green PCR Master Mix (Applied Biosystems) in a total volume of 20 μL. For each biological sample, qPCR reactions were performed in triplicate on an Applied Biosystems Prism 7500HT Sequence Detection System. Baseline values of amplification plots were set automatically and threshold values were kept constant to obtain normalized cycle times and linear regression data. Individual receptor PCR efficiencies were calculated from the slope of the resulting standard curves using the following formula: $E = 10\text{-}1/slope$, where E is efficiency.[5,6] Indeed, the obtained efficiency was used to convert cycle times from log to linear scale using the following formula: $E - cycle\ threshold$. Normalized mRNA levels are expressed as arbitrary units and were obtained by dividing the averaged, efficiency-corrected values for NR mRNA expression by that of cyclophilin mRNA expression for each sample. The resulting values were multiplied by 106 for graphic representation and plotted as mean ± SEM of 6 HT29 APC inducible cells, 12 $Apc^{Min/+}$ mice, and 10 FAP patient samples. For $Apc^{Min/+}$ mice, normalized mRNA expression levels were defined as follows: absent, if the arbitrary units were less than 0.1, low if the arbitrary units were between 0.1 and 8.9, moderate if the arbitrary units were between 8.9 and 1331.2, and high if the arbitrary units were greater than 1331.2. For FAP patients, normalized mRNA expression levels were defined as follows: absent, if the arbitrary units were less than 55.8, low if the arbitrary units were between 55.8 and 3048.3, moderate if the arbitrary units were between 3048.3 and 452,411.4, and high if the arbitrary units were greater than 452,411.4. For HT29-APC inducible cells, normalized mRNA expression levels were defined as follows: absent, if the arbitrary units were less than 1.0, low if the arbitrary units were between 1.0 and 54.0, moderate if the arbitrary units were between 54.0 and 8029.0, and high if the arbitrary units were greater than 8029.0. The arbitrary units used to define the mRNA expression levels were obtained from the formulas described earlier assuming a cycle threshold of 34 or greater for absent, 34 to 30 for low, less than 30 to 26 for moderate, and 25 or less for high expression.

Supplementary References

1. Wu G, Wu W, Hegde M, et al. Detection of sequence variations in the adenomatous polyposis coli (APC) gene using denaturing high-performance liquid chromatography. Genet Test 2001;5:281–290.
2. Aceto G, Cristina CM, Veschi S, et al. Mutations of APC and MYH in unrelated Italian patients with adenomatous polyposis coli. Hum Mutat 2005;26:394.
3. Morin PJ, Vogelstein B, Kinzler KW. Apoptosis and APC in colorectal tumorigenesis. Proc Natl Acad Sci U S A 1996;93:7950–7954.
4. Gofflot F, Chartoire N, Vasseur L, et al. Systematic gene expression mapping clusters nuclear receptors according to their function in the brain. Cell 2007;131:405–418.
5. Bookout AL, Jeong Y, Downes M, et al. Anatomical profiling of nuclear receptor expression reveals a hierarchical transcriptional network. Cell 2006;126:789–799.
6. Yang X, Downes M, Yu RT, et al. Nuclear receptor expression links the circadian clock to metabolism. Cell 2006;126:801–810.

Supplementary Table 1. Detailed Information on the ISH Probes Used in the Study

Name		Template	Origin	Sequence data	Study
NR1A1	Trα	pdrive	Mark M, IGBMC, Strasbourg, France, marek@igbmc.u-strasbg.fr	5′ bp location: 729-3′ bp location: 1185 (456 bp of LBD)	Unpublished data
NR1A2	Trβ	pdrive	Mark M, IGBMC, Strasbourg, France, marek@igbmc.u-strasbg.fr	5′ bp location: 621-3′bp location: 1085 (465 bp of exons 2 ,3, and 4)	Unpublished data
NR1B1	Rarα	Plasmid BMS13+	Dolle P and Chambon P, IGBMC, Strasbourg, France, dolle@igbmc.fr	1.6 kb insert of cDNA corresponding to whole ORF	Zelent et al
NR1B2	Rarβ	Plasmid BMS13+	Dolle P and Chambon P, IGBMC, Strasbourg, France, dolle@igbmc.fr	1.7 kb insert of cDNA corresponding to whole ORF	Zelent et al
NR1B3	Rarγ	Plasmid SG5	Dolle P and Chambon P, IGBMC, Strasbourg, France, dolle@igbmc.fr	1.9 kb insert of cDNA corresponding to whole ORF	Zelent et al
NR1C1	Pparα	Template PCR	Genepaint, http://www.genepaint.org	http://www.genepaint.org/cgi-bin/mgrqcgi94?APPNAME=genepaint&PRGNAME=r na_probe_show&ARGUMENTS=AQ86545035742805,-Ashow:MH,-A670	Visel et al
NR1C2	Pparδ	Plasmid PSK	Qiufu Ma, Dana-Farber Cancer Institute, Boston, MA, Qiufu_Ma@dfci.harvard.edu	5′ bp location: 421-3′bp location: 1183	Gray et al
NR1C3	Pparγ	Template PCR	Genepaint, http://www.genepaint.org	http://www.genepaint.org/cgi-bin/mgrqcgi94?APPNAME=genepaint&PRGNAME=r na_probe_show&ARGUMENTS=AQ33443994320500,-Ashow:EH,-A3489	Visel et al
NR1D1	RevErbα	Plasmid PCRII	Qiufu Ma, Dana-Farber Cancer Institute, Boston, MA, Qiufu_Ma@dfci.harvard.edu	5′ bp location: 334 - 3′bp location: 1044	Gray et al
NR1D2	RevErbβ	Template PCR	Genepaint, http://www.genepaint.org	http://www.genepaint.org/cgi-bin/mgrqcgi94?APPNAME=genepaint&PRGNAME=r na_probe_show&ARGUMENTS=AQ02097875871607,-Ashow:MH,-A438	Visel et al
NR1F1	Rorα	Template PCR	Genepaint, http://www.genepaint.org	http://www.genepaint.org/cgi-bin/mgrqcgi94?APPNAME=genepaint&PRGNAME=r na_probe_show&ARGUMENTS=AQ48920297265409,-Ashow:EH,-A3723	Visel et al
NR1F2	Rorβ	Template PCR	Genepaint, http://www.genepaint.org	http://www.genepaint.org/cgi-bin/mgrqcgi94?APPNAME=genepaint&PRGNAME=r na_probe_show&ARGUMENTS=AQ29252046915808,-Ashow:MH,-A241	Visel et al
NR1F3	Rorγ	Plasmid PSK	Qiufu Ma, Dana-Farber Cancer Institute, Boston, MA, Qiufu_Ma@dfci.harvard.edu	5′ bp location: 961-3′bp location: 1745	Gray et al
NR1H2	Lxrβ	Plasmid pBSKS+	Auwerx J, IGBMC, Strasbourg, France, auwerx@igbmc.u-strasbg.fr	Mouse Lxrβ full ORF	Repa et al
NR1H3	Lxrα	Plasmid pBSSK+	Auwerx J, IGBMC, Strasbourg, France, auwerx@igbmc.u-strasbg.fr	Mouse Lxrα full ORF	Repa et al
NR1H4	Fxrα	Plasmid pBSKS+	Auwerx J, IGBMC, Strasbourg, France, auwerx@igbmc.u-strasbg.fr	Mouse Fxrα4 (β2) full ORF 1.6 kb	Houten et al
NR1H5	Fxrβ	pdrive	Auwerx J, IGBMC, Strasbourg, France, auwerx@igbmc.u-strasbg.fr	777 bp insert cDNA corresponding to exon1	Gofflot et al
NR1I1	Vdr	Plasmid	Dolle P, IGBMC, Strasbourg, France, dolle@igbmc.fr		Shigeaki Kato (The University of Tokyo, Tokyo, Japan)
NR1I2	Pxr	Plasmid pBSKS+	Auwerx J, IGBMC, Strasbourg, France, auwerx@igbmc.u-strasbg.fr	Mouse Pxr full ORF1.2 kb	Cloned by Sander Houten, unpublished data
NR1I3	Car	Template PCR	Genepaint, http://www.genepaint.org	http://www.genepaint.org/cgi-bin/mgrqcgi94?APPNAME=genepaint&PRGNAME=r na_probe_show&ARGUMENTS=AQ65658406610408,-Ashow:EH,-A2542	Visel et al
NR2A1	Hnf4α	Template PCR	Genepaint, http://www.genepaint.org	http://www.genepaint.org/cgi-bin/mgrqcgi94?APPNAME=genepaint&PRGNAME=r na_probe_show&ARGUMENTS=AQ59982144504903,-Ashow: EG,-A1233	Visel et al
NR2A2	Hnf4γ	Plasmid PCRII	Qiufu Ma, Dana-Farber Cancer Institute, Boston, USA, Qiufu_Ma@dfci.harvard.edu	5′ bp location: 361-3′bp location: 1113	Gray et al
NR2B1	Rxrα	Plasmid BSK+	Dolle P and Chambon P, IGBMC, Strasbourg, France, dolle@igbmc.fr	Mouse Rxrα full ORF – 1.4kb	Dolle et al
NR2B2	Rxrβ	Plasmid BSK+	Dolle P and Chambon P, IGBMC, Strasbourg, France, dolle@igbmc.fr	Mouse Rxrβ full ORF – 1.3kb	Dolle et al
NR2B3	Rxrγ	Plasmid	Dolle P and Chambon P, IGBMC, Strasbourg, France, dolle@igbmc.fr	Mouse Rxrγ full ORF – 1.4kb	Dolle et al
NR2C1	Tr2	Template PCR	Genepaint, http://www.genepaint.org	http://www.genepaint.org/cgi-bin/mgrqcgi94?APPNAME=genepaint&PRGNAME=r na_probe_show&ARGUMENTS=AQ40662404369504,-Ashow:MH,-A916	Visel et al
NR2C2	Tr4	pdrive	Auwerx J, IGBMC, Strasbourg, France, auwerx@igbmc.u-strasbg.fr	747 bp insert cDNA corresponding to exon1	Gofflot et al

Supplementary Table 1. Continued

Name		Template	Origin	Sequence data	Study
NR2E1	Tlx	Template PCR	Genepaint, http://www.genepaint.org	http://www.genepaint.org/cgi-bin/mgrqcgi94?APPNAME=genepaint&PRGNAME=r na_probe_show&ARGUMENTS=AQ24149449768206,-Ashow:MH,-A711	Visel et al
NR2E3	Pnr	Plasmid PCRII	Qiufu Ma, Dana-Farber Cancer Institute, Boston, MA, Qiufu_Ma@dfci.harvard.edu	5′ bp location: 301-3′bp location: 1044	Gray et al
NR2F1	Coup-TFI	Plasmid BSII-KS+	Dolle P, IGBMC, Strasbourg, France, dolle@igbmc.fr	600 bp of 3′ UTR of mCOUP-TFI	Qiu et al
NR2F2	Coup-TFII	Plasmid BSII-KS+	Dolle P, IGBMC, Strasbourg, France, dolle@igbmc.fr	1000 bp of 3′ UTR of mCOUP-TFII	Qiu et al
NR2F6	Ear2	Template PCR	Genepaint, http://www.genepaint.org	http://www.genepaint.org/cgi-bin/mgrqcgi94?APPNAME=genepaint&PRGNAME=r na_probe_show&ARGUMENTS=AQ28225862645703,-Ashow:MH,-A109	Visel et al
NR3A1	Erα	Plasmid BSKII	Krust A and Chambon P, IGBMC, Strasbourg, France, Andree.KRUST@igbmc.fr	Mouse Erα full ORF-1.9kb	Unpublished data
NR3A2	Erβ	Plasmid BSK	Krust A and Chambon P, IGBMC, Strasbourg, France, Andree.KRUST@igbmc.fr	Mouse Erβ full ORF-1.65kb	Unpublished
NR3B1	Errα	Template PCR	Genepaint, http://www.genepaint.org	http://www.genepaint.org/cgi-bin/mgrqcgi94?APPNAME=genepaint&PRGNAME=r na_probe_show&ARGUMENTS=AQ81532902980907,-Ashow:MH,-A712	Visel et al
NR3B2	Errβ	Template PCR	Genepaint, http://www.genepaint.org	http://www.genepaint.org/cgi-bin/mgrqcgi94?APPNAME=genepaint&PRGNAME=r na_probe_show&ARGUMENTS=AQ81532902980907,-Ashow:MH,-A713	Visel et al
NR3B3	Errγ	Plasmid	Auwerx J, IGBMC, Strasbourg, France, auwerx@igbmc.u-strasbg.fr	mouse Errγ full ORF 1.6 kb	Cloned by Hiroyuki or MGC (commercial), unpublished data
NR3C1	Gr	Plasmid PCRII	Qiufu Ma, Dana-Farber Cancer Institute, Boston, MA, Qiufu_Ma@dfci.harvard.edu	5′ bp location: 512-3′bp location: 1312	Gray et al
NR3C2	Mr	Plasmid PSK	Qiufu Ma, Dana-Farber Cancer Institute, Boston, MA, Qiufu_Ma@dfci.harvard.edu	5′ bp location: 297-3′bp location: 1079	Gray et al
NR3C3	Pr	Plasmid PCRII	Qiufu Ma, Dana-Farber Cancer Institute, Boston, MA, Qiufu_Ma@dfci.harvard.edu	5′ bp location: 730-3′bp location: 1545	Gray et al
NR3C4	Ar	Template PCR	Genepaint, http://www.genepaint.org	http://www.genepaint.org/cgi-bin/mgrqcgi94?APPNAME=genepaint&PRGNAME=r na_probe_show&ARGUMENTS=AQ04051916779208,-Ashow:MH,-A874	Visel et al
NR4A1	NgfIB	Plasmid PSK	Qiufu Ma, Dana-Farber Cancer Institute, Boston, MA, Qiufu_Ma@dfci.harvard.edu	5′ bp location: 779-3′bp location: 1525	Gray et al
NR4A2	Nurr1	Plasmid PSK	Qiufu Ma, Dana-Farber Cancer Institute, Boston, MA, Qiufu_Ma@dfci.harvard.edu	5′ bp location: 816-3′bp location: 1703	Gray et al
NR4A3	Nor1	Plasmid PSK	Qiufu Ma, Dana-Farber Cancer Institute, Boston, MA, Qiufu_Ma@dfci.harvard.edu	5′ bp location: 421-3′bp location: 1165	Gray et al
NR5A1	Sf-1	Plasmid pBSSK+	Auwerx J, IGBMC, Strasbourg, France, auwerx@igbmc.u-strasbg.fr	Mouse Sf-1 full ORF 2 kb	Keith Parker (Departments of Internal Medicine and Pharmacology, UT Southwestern Medical Center, Dallas, TX)
NR5A2	Lrh-1	Plasmid pBSSK+	Auwerx J, IGBMC, Strasbourg, France, auwerx@igbmc.u-strasbg.fr	Mouse Lrh-1 full ORF 1.6 kb	Fayard et al
NR6A1	Gcnf	pBluescript II SK	Austin Cooney, Baylor, Houston, TX	1.95 kb of Gcnf cDNA	Katz et al
NR0B1	Dax1	Template PCR	Genepaint, http://www.genepaint.org	http://www.genepaint.org/cgi-bin/mgrqcgi94?APPNAME=genepaint&PRGNAME=r na_probe_show&ARGUMENTS=AQ29871925059503,-Ashow:MH,-A917	Visel et al
NR0B2	Shp	Plasmid pBSSK+	Auwerx J., IGBMC, Strasbourg, France, auwerx@igbmc.u-strasbg.fr	Mouse SHP full ORF 1.2 kb	Watanabe et al

NOTE. Further info can be obtained at http://www-mci.u-strasbg.fr/mousepat/.

Supplementary Table 2. ISH Intensity Values of NR Transcripts in Normal Mouse Intestine

Gene name		Colon			Ileum		
Trivial	Official	*E*	*C*	Pattern	*V*	*C*	Pattern
Trα	NR1A1	0	0.5	C	0	2	C
Trβ	NR1A2	0	0.5	C	0.5	0.5	U
Rarα	NR1B1	2	3	U	3	3	U
Rarβ	NR1B2	1	1	U	1	1	U
Rarγ	NR1B3	1.5	2.5	C	2	2	U
Pparα	NR1C1	1	1	U	0.5	1	U
Pparδ	NR1C2	1	2	C	1	3	C
Pparγ	NR1C3	1	3	C	1.5	1.5	U
Rev-erbα	NR1D1	0.5	0.5	U	1.5	0	V
Rev-erbβ	NR1D2	0.5	0.5	U	1.5	0	V
Rorα	NR1F1	0	0	ND	0.5	0	ND
Rorβ	NR1F2	0	0	ND	0	0	ND
Rorγ[a]	NR1F3	0	1	C	1	0.5	U
Lxrα[a]	NR1H3	1.5	0.5	E	1.5	0.5	V
Lxrβ	NR1H2	2	2	U	2	2	U
Fxrα	NR1H4	3	0	E	3	0	V
Fxrβ[a]	NR1H5	0.5	0.5	ND	0.5	0	ND
Vdr	NR1I1	3	2	E	3	1	V
Pxr	NR1I2	2	0.5	E	2	1	V
Car	NR1I3	0.5	0.5	U	0.5	0.5	U
Hnf4α	NR2A1	3	2	E	3	1	V
Hnf4γ	NR2A2	0.5	0.5	U	2	0.5	V
Rxrα	NR2B1	3	2	E	3	1	V
Rxrβ	NR2B2	0.5	3	C	1.5	2	U
Rxrγ[a]	NR2B3	0	1	C	0.5	0.5	U
Tr2	NR2C1	0	0	ND	0	0	ND
Tr4	NR2C2	0.5	0.5	U	1	0	V
Tlx	NR2E2	0	0	ND	0.5	0	ND
Pnr	NR2E3	0	0	ND	0	0	ND
Coup-TFI	NR2F1	0	0.5	C	0.5	1	C
Coup-TFII	NR2F2	0	1	C	1	2.5	C
Ear2	NR2F6	0.5	2	C	2	1.5	V
Erα	NR3A1	0.5	0.5	U	0.5	1	U
Erβ	NR3A2	0.5	0	E	0.5	0	V
Errα	NR3B1	3	1.5	E	3	0.5	V
Errβ[a]	NR3B2	0	0	ND	0.5	0.5	U
Errγ	NR3B3	0.5	0.5	U	0.5	0.5	U
Gr	NR3C1	2	0.5	E	3	1	V
Mr	NR3C2	3	0.5	E	3	0	V
Pr	NR3C3	0	0	ND	0.5	0	ND
Ar	NR3C4	0	0	ND	0.5	0	ND
NgfIB[a]	NR4A1	0.5	1.5	C	0.5	1	C
Nurr1[a]	NR4A2	0.5	2.5	C	0.5	1.5	C
Nor1	NR4A3	0	1	C	0.5	1	C
Sf1	NR5A1	0	0	ND	0	0	ND
Lrh1	NR5A2	0.5	3	C	1	3	C
Gcnf1	NR6A1	0.5	1	U	1	1	U
Dax	NR0B1	0	0	ND	0	0	ND
Shp	NR0B3	0	0.5	ND	0.5	0	ND

NOTE. Intensity: from 3 (maximal) to 0.5 (background level). ND (not detectable) refers to the absence of signal in the intestinal epithelium, but does not exclude the presence of signal in submucosal layers, endocrine cells, lymphoid, and mesenchymal cells.

C, crypt; E, upper third of the crypt-epithelium; ND, not detectable; U, ubiquitous; V, villus.

[a]These genes are (solely or additionally) expressed in scattered cells within the epithelium that may correspond to specific cell types (eg, endocrine or macrophages) and this particular expression thus was not taken into account for the annotation. Details on anatomic distribution and compartment divisions are reported in Supplementary Figure 6 legend.

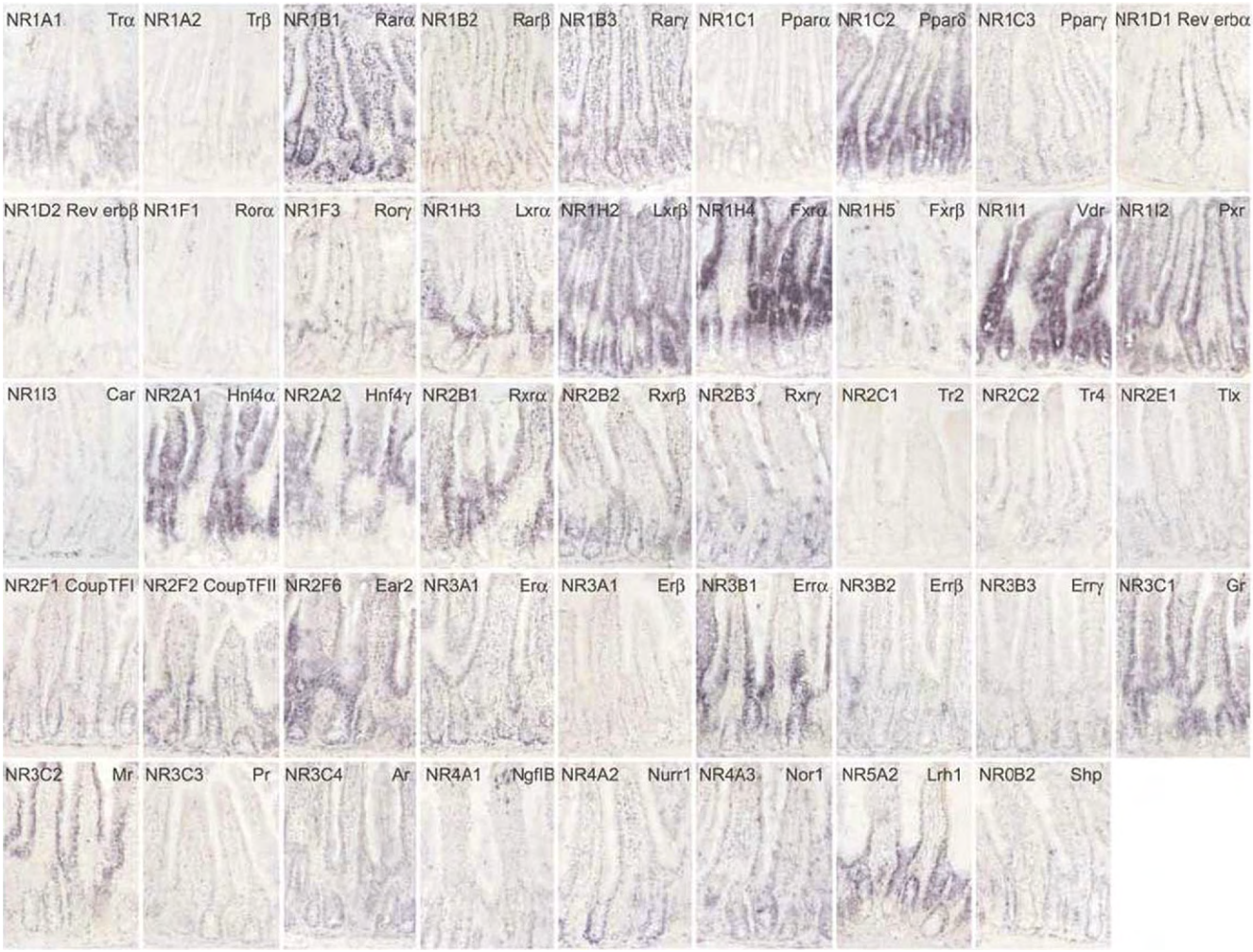

Supplementary Figure 1. NR nonradioactive ISH on mouse ileum. Spatial distribution of NR transcripts in normal mouse ileum (villus, crypt, ubiquitous) using nonradioactive ISH. Only NR transcripts with intensity between 3 (maximal) and 0.5 (background) are shown.

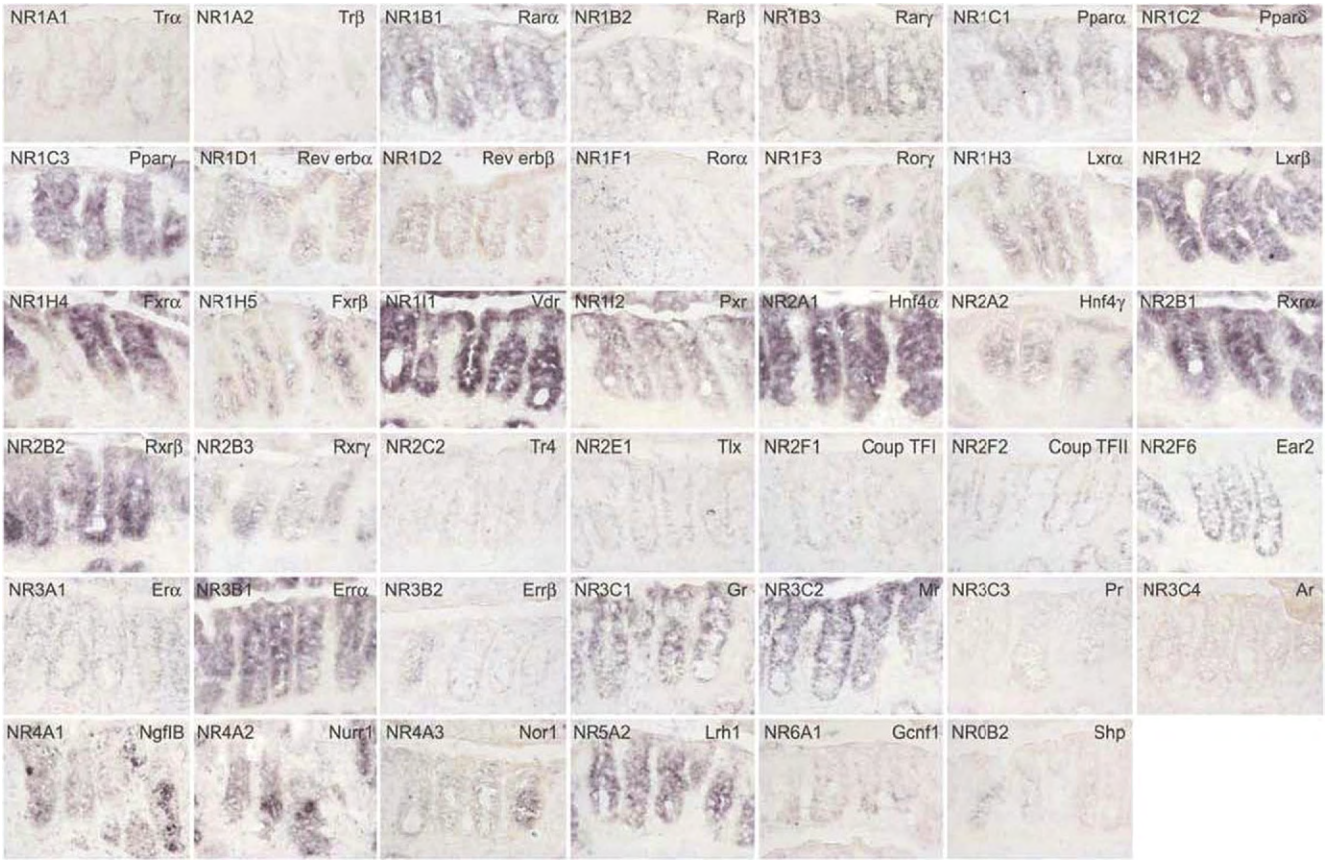

Supplementary Figure 2. NR nonradioactive ISH on mouse colon. Spatial distribution of NR transcripts in normal mouse colon (epithelium, crypt, ubiquitous) using nonradioactive ISH. Only NR transcripts with intensity between 3 (maximal) and 0.5 (background) are shown.

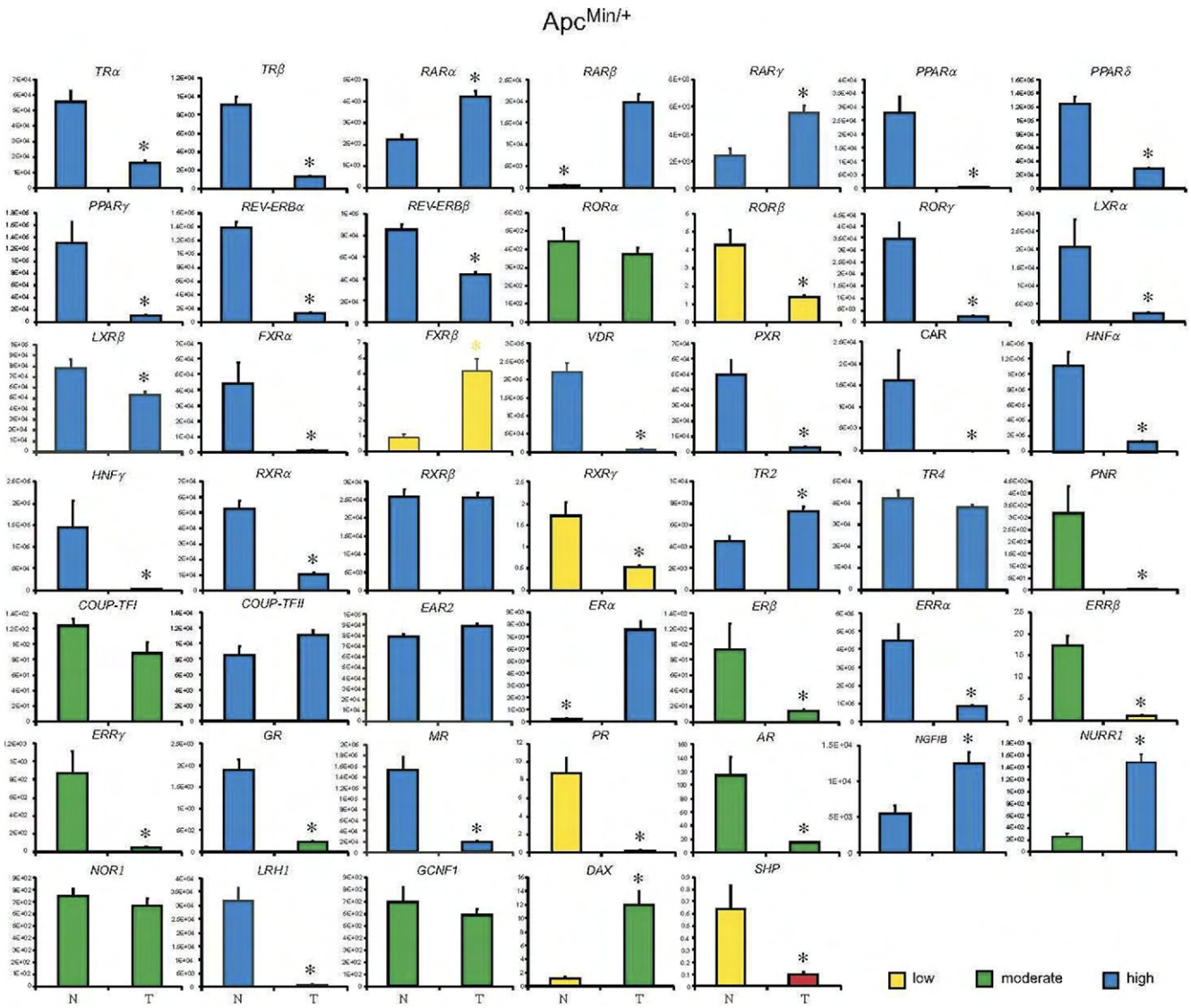

Supplementary Figure 3. Profile of the NR transcriptome in the colon of a mouse model of CRC. NR expression levels in colon tumors of ApcMin/+ mice are compared with normal adjacent regions. Genes are represented in 4 different colors based on their expression levels (*red*, *yellow*, *green*, and *blue* for absent, low, moderate, and high expression, respectively). Genes that are classified as absent in both tumors and adjacent normal regions are not shown. Values are expressed as relative units and plotted as the mean ± SEM of 12 mice. *P* values for significant differences are reported in Supplementary Table 2.

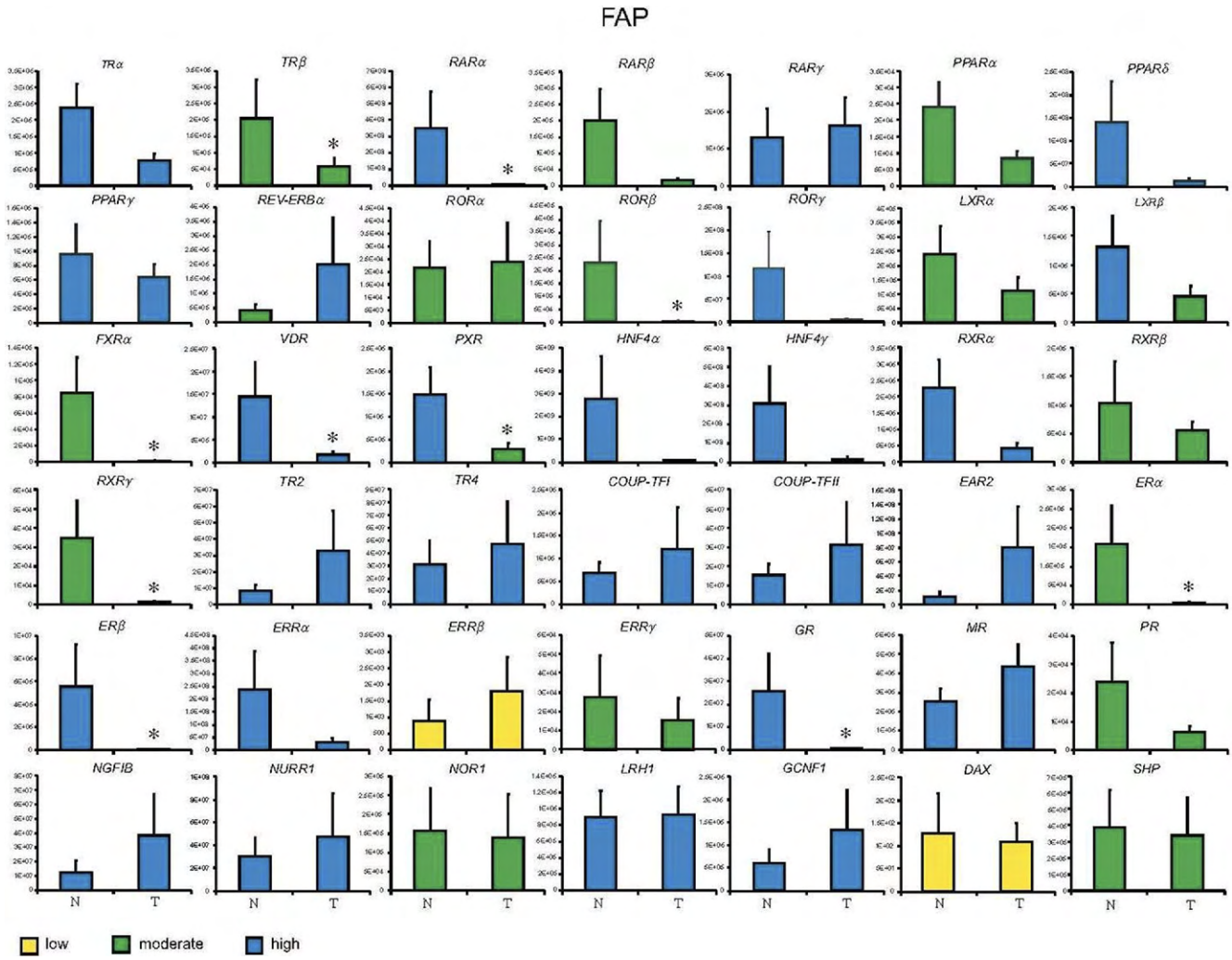

Supplementary Figure 4. Profile of the NR transcriptome in the colon of a human model of CRC. NR expression levels in colon tumors of FAP patients are compared with normal adjacent regions. Genes are represented in 3 different colors based on their expression levels (*yellow*, *green*, and *blue* for low, moderate, and high expression, respectively). Genes that are classified as absent in both tumors and adjacent normal regions are not shown. Values are expressed as relative units and plotted as the mean ± SEM of 10 patients. *P* values for significant differences are reported in Supplementary Table 2.

Supplementary Table 3. Normalized Expression Levels of Each NR in the 3 Different Models of APC Initiated Colon Tumors

Name		ApcMin/+ mice			FAP patients			HT29 APCi cells		
Trivial	Official	Normal	Tumor	*P*	Normal	Tumor	*P*	− ZnCl2	+ ZnCl2	*P*
TRα	NR1A1	5.50E + 04 ± 0.24E + 03	1.59E + 04 ± 1.53E + 03	.001	2.39E + 06 ± 7.52E + 05	7.53E + 05 ± 2.32E + 05	.062	1.41E + 05 ± 2.21E + 04	6.51E + 04 ± 9.18E + 03	.062
TRβ	NR1A2	9.46E + 03 ± 8.41E + 02	1.34E + 03 ± 1.17E + 02	.001	2.05E + 05 ± 1.19E + 05	6.04E + 04 ± 2.33E + 04	.695	1.94E + 03 ± 3.12E + 02	6.05E + 03 ± 7.33E + 02	.062
RARα	NR1B1	2.32E + 03 ± 2.08E + 02	4.36E + 03 ± 2.32E + 02	.001	3.56E + 08 ± 2.26E + 08	3.60E + 06 ± 9.16E + 05	.003	1.37E + 05 ± 1.91E + 04	6.45E + 05 ± 6.77E + 04	.031
RARβ	NR1B2	5.15E + 02 ± 9.44E + 01	2.01E + 04 ± 1.91E + 03	.001	2.01E + 05 ± 9.67E + 04	1.78E + 04 ± 5.95E + 03	.062	4.09E − 02 ± 2.19E − 02	9.65E − 01 ± 3.15E − 01	.062
RARγ	NR1B3	2.40E + 03 ± 5.82E + 02	5.58E + 03 ± 5.51E + 02	.001	1.31E + 06 ± 7.59E + 05	1.62E + 06 ± 7.72E + 05	1	5.66E + 05 ± 9.65E + 04	6.68E + 05 ± 8.26E + 04	1
PPARα	NR1C1	2.78E + 04 ± 6.11E + 03	2.29E + 02 ± 8.18E + 00	.001	2.43E + 04 ± 7.40E + 03	8.31E + 03 ± 2.41E + 03	.167	7.22E + 03 ± 1.68E + 03	5.62E + 03 ± 6.90E + 02	.562
PPARδ	NR1C2	1.24E + 05 ± 1.07E + 04	2.96E + 04 ± 1.52E + 03	.001	1.40E + 08 ± 9.09E + 07	1.12E + 07 ± 6.72E + 06	.083	1.20E + 05 ± 1.70E + 04	1.00E + 06 ± 1.21E + 05	.062
PPARγ	NR1C3	1.29E + 05 ± 3.48E + 04	1.03E + 04 ± 9.33E + 02	.036	9.55E + 05 ± 4.25E + 05	6.28E + 05 ± 1.94E + 05	.921	1.52E + 06 ± 2.88E + 05	4.01E + 06 ± 6.20E + 05	.062
REVERB α	NR1D1	1.37E + 05 ± 8.40E + 03	1.27E + 04 ± 8.77E + 02	.001	3.93E + 05 ± 2.32E + 05	2.05E + 06 ± 1.63E + 06	.695	5.51E + 06 ± 1.15E + 06	1.31E + 07 ± 3.71E + 06	.625
REVERB β	NR1D2	8.52E + 04 ± 4.68E + 03	4.44E + 04 ± 1.90E + 03	.001	ND	ND		6.07E + 00 ± 1.52E + 00	8.96E + 00 ± 2.93E + 00	.687
RORα	NR1F1	4.53E + 02 ± 6.75E + 01	3.78E + 02 ± 3.78E + 01	.276	2.17E + 04 ± 1.06E + 04	2.39E + 04 ± 1.54E + 04	.492	6.14E + 00 ± 1.48E + 00	8.84E + 00 ± 1.21E + 00	.276
RORβ	NR1F2	4.32E + 00 ± 8.34E − 01	1.39E + 00 ± 9.13E − 02	.001	2.30E + 05 ± 1.61E + 05	3.08E + 03 ± 1.53E + 03	.019	8.64E − 01 ± 2.72E − 01	1.81E + 01 ± 1.83E + 00	.031
RORγ	NR1F3	3.51E + 04 ± 6.99E + 03	2.51E + 03 ± 2.65E + 02	.001	1.15E + 08 ± 7.87E + 07	4.76E + 06 ± 2.63E + 06	.187	2.84E + 02 ± 6.65E + 01	1.50E + 02 ± 1.94E + 01	.187
LXRα	NR1H3	2.07E + 04 ± 7.53E + 03	2.47E + 03 ± 9.40E + 01	.001	2.39E + 05 ± 1.01E + 05	1.13E + 05 ± 4.36E + 04	.984	3.39E + 05 ± 7.50E + 04	3.55E + 05 ± 5.47E + 04	.984
LXRβ	NR1H2	7.73E + 04 ± 8.43E + 03	5.33E + 04 ± 2.90E + 03	.014	1.32E + 06 ± 5.27E + 05	4.52E + 05 ± 1.78E + 05	.320	5.33E + 05 ± 1.05E + 05	7.81E + 05 ± 1.43E + 05	.320
FXRα	NR1H4	4.40E + 04 ± 1.38E + 04	8.67E + 02 ± 8.45E + 01	.001	6.28E + 04 ± 3.97E + 04	2.85E + 03 ± 1.34E + 03	.003	1.60E + 01 ± 2.37E + 00	1.66E + 02 ± 1.91E + 01	.031
FXRβ	NR1H5	8.84E − 01 ± 2.12E − 01	5.09E + 00 ± 7.71E − 01	.001	ND	ND		ND	ND	
VDR	NR1I1	2.19E + 05 ± 2.56E + 04	5.77E + 03 ± 6.44E + 02	.001	1.45E + 07 ± 7.48E + 06	1.67E + 06 ± 6.95E + 05	.019	1.35E + 06 ± 2.61E + 05	4.95E + 06 ± 1.33E + 06	.156
PXR	NR1I2	5.01E + 04 ± 9.30E + 03	3.02E + 03 ± 2.64E + 02	.001	1.50E + 06 ± 5.98E + 05	2.96E + 05 ± 1.24E + 05	.019	3.43E + 01 ± 6.17E + 00	6.21E + 01 ± 1.24E + 01	.218
CAR	NR1I3	1.59E + 04 ± 6.72E + 03	9.27E + 00 ± 1.54E + 00	.001	ND	ND		7.47E − 03 ± 2.76E − 03	1.11E + 01 ± 2.32E + 00	.031
HNF4α	NR2A1	1.11E + 06 ± 1.82E + 05	1.34E + 05 ± 7.60E + 03	.001	2.77E + 09 ± 1.86E + 09	6.27E + 07 ± 3.24E + 07	.062	1.14E + 05 ± 1.75E + 04	2.86E + 04 ± 3.16E + 03	.062
HNF4γ	NR2A2	1.45E + 05 ± 6.10E + 04	1.27E + 03 ± 8.25E + 01	.001	3.09E + 08 ± 1.91E + 08	1.73E + 07 ± 1.01E + 07	.083	1.76E + 05 ± 2.56E + 04	6.52E + 04 ± 8.08E + 03	.062
RXRα	NR2B1	5.31E + 04 ± 4.99E + 03	1.01E + 04 ± 4.54E + 02	.001	2.28E + 06 ± 8.65E + 05	4.31E + 05 ± 1.51E + 05	.054	1.60E + 06 ± 2.83E + 05	1.13E + 06 ± 1.80E + 05	.312
RXRβ	NR2B2	2.61E + 04 ± 1.91E + 03	2.59E + 04 ± 1.24E + 03	1	1.05E + 05 ± 7.31E + 04	5.52E + 04 ± 1.65E + 04	1	5.63E + 05 ± 1.39E + 05	4.03E + 05 ± 4.80E + 04	1
RXRγ	NR2B3	1.72E + 00 ± 3.04E − 01	5.27E − 01 ± 5.37E − 02	.041	3.49E + 04 ± 1.94E + 04	9.31E + 02 ± 3.95E + 02	.011	4.92E − 01 ± 1.87E − 01	1.94E + 01 ± 3.99E + 00	.041
TR2	NR2C1	4.54E + 03 ± 4.65E + 02	7.31E + 03 ± 3.55E + 02	.001	8.26E + 06 ± 4.33E + 06	3.29E + 07 ± 2.46E + 07	1	9.86E + 04 ± 1.32E + 04	1.28E + 05 ± 9.57E + 03	.437
TR4	NR2C2	4.24E + 04 ± 3.72E + 03	3.82E + 04 ± 1.43E + 03	.454	3.13E + 07 ± 1.88E + 07	4.73E + 07 ± 3.41E + 07	1	4.31E + 06 ± 9.07E + 05	3.44E + 06 ± 9.41E + 05	.437
TLX	NR2E1	ND	ND		ND	ND		5.90E − 01 ± 1.80E − 01	6.43E + 02 ± 1.80E + 02	.031
PNR	NR2E3	3.14E + 02 ± 1.13E + 02	3.53E + 00 ± 4.81E − 01	.001	ND	ND		4.36E − 01 ± 5.36E − 02	1.80E + 00 ± 4.62E − 01	.031
COUPTFI	NR2F1	1.23E + 02 ± 9.34E + 00	8.82E + 01 ± 1.45E + 01	.102	6.79E + 05 ± 2.40E + 05	1.20E + 06 ± 9.22E + 05	.320	6.86E + 06 ± 2.59E + 06	3.86E + 06 ± 1.21E + 06	.687
COUPTFII	NR2F2	8.43E + 03 ± 1.14E + 03	1.11E + 04 ± 5.49E + 02	.231	1.55E + 07 ± 5.65E + 06	3.10E + 07 ± 2.26E + 07	1	9.07E + 07 ± 2.80E + 07	4.99E + 07 ± 3.01E + 07	1
EAR2	NR2F6	7.80E + 04 ± 2.03E + 03	8.68E + 04 ± 2.24E + 03	.127	1.13E + 07 ± 6.33E + 06	7.92E + 07 ± 5.75E + 07	1	6.40E + 07 ± 2.33E + 07	3.62E + 07 ± 1.18E + 07	1
ERα	NR3A1	1.66E + 02 ± .76E + 01	7.53E + 03 ± 7.24E + 02	.001	1.59E + 05 ± 1.02E + 05	4.15E + 03 ± 1.74E + 03	.003	1.78E − 02 ± 5.51E − 03	2.81E − 01 ± 3.88E − 02	.031
ERβ	NR3A2	9.30E + 01 ± 3.43E + 01	1.46E + 01 ± 1.36E + 00	.041	5.65E + 06 ± 3.70E + 06	6.81E + 04 ± 2.43E + 04	.005	1.82E + 00 ± 3.25E − 01	8.90E + 02 ± 1.10E + 02	.041
ERRα	NR3B1	4.46E + 05 ± 9.62E + 04	8.59E + 04 ± 3.64E + 03	.001	2.37E + 08 ± 1.53E + 08	2.87E + 07 ± 1.75E + 07	.167	6.03E + 05 ± 9.36E + 04	4.98E + 05 ± 5.45E + 04	.562
ERRβ	NR3B2	1.74E + 01 ± 2.21E + 00	1.07E + 00 ± 1.56E − 01	.001	8.87E + 02 ± 6.68E + 02	1.81E + 03 ± 1.05E + 03	.275	8.35E + 00 ± 2.39E + 00	1.82E + 02 ± 2.02E + 01	.062
ERRγ	NR3B3	8.67E + 02 ± 2.40E + 02	4.53E + 01 ± 8.76E + 00	.001	2.76E + 04 ± 2.14E + 04	1.54E + 04 ± 1.14E + 04	1	2.05E + 00 ± 1.73E − 01	7.23E − 01 ± 9.06E − 02	.062
GR	NR3C1	1.88E + 03 ± 2.49E + 02	2.25E + 02 ± 1.07E + 01	.001	2.63E + 07 ± 1.63E + 07	7.30E + 05 ± 2.13E + 05	.007	1.51E − 02 ± 8.25E − 03	3.17E + 01 ± 3.35E + 00	.031
MR	NR3C2	1.51E + 05 ± 2.43E + 04	1.79E + 04 ± 1.57E + 03	.001	2.54E + 06 ± 7.04E + 05	4.39E + 06 ± 1.17E + 06	.322	2.63E + 02 ± 4.47E + 01	1.25E + 03 ± 1.72E + 02	.062
PR	NR3C3	8.72E + 00 ± 1.75E + 00	1.63E − 01 ± 2.25E − 02	.001	2.43E + 04 ± 1.37E + 04	6.33E + 03 ± 1.93E + 03	.105	5.79E − 02 ± 1.95E − 02	1.72E + 00 ± 5.74E − 01	.062
AR	NR3C4	1.13E + 02 ± 2.65E + 01	1.53E + 01 ± 8.19E − 01	.001	ND	ND		ND	ND	
NGFIB	NR4A1	5.48E + 03 ± 1.11E + 03	1.25E + 04 ± 1.54E + 03	.014	1.20E + 07 ± 8.32E + 06	3.83E + 07 ± 2.87E + 07	.431	1.34E + 04 ± 2.67E + 03	3.72E + 05 ± 9.88E + 04	.062
NURR1	NR4A2	2.50E + 02 ± 5.01E + 01	1.48E + 03 ± 1.26E + 02	.001	3.04E + 07 ± 1.60E + 07	4.75E + 07 ± 3.77E + 07	.556	2.41E + 06 ± 8.88E + 05	1.70E + 07 ± 4.90E + 06	.062
NOR1	NR4A3	7.53E + 02 ± 5.90E + 01	6.71E + 02 ± 5.75E + 01	.850	1.57E + 05 ± 1.57E + 05	1.40E + 05 ± 1.14E + 05	.750	2.54E + 04 ± 5.46E + 03	1.07E + 06 ± 3.24E + 05	.093
SF1	NR5A1	3.47E − 02 ± 1.46E − 02	1.43E − 02 ± 2.52E − 03	.850	ND	ND		5.85E + 01 ± 7.03E + 00	3.56E + 01 ± 1.04E + 01	.437
LRH1	NR5A2	3.16E + 04 ± 4.83E + 03	5.00E + 02 ± 5.87E + 01	.001	9.07E + 05 ± 3.21E + 05	9.30E + 05 ± 3.45E + 05	1	2.28E + 03 ± 3.64E + 02	2.06E + 03 ± 2.46E + 02	1
GCNF1	NR6A1	6.94E + 02 ± 1.23E + 02	5.89E + 02 ± 5.11E + 01	1	6.06E + 05 ± 3.00E + 05	1.34E + 06 ± 8.59E + 05	1	1.75E + 04 ± 3.04E + 03	8.05E + 03 ± 1.16E + 03	.187
DAX	NR0B1	1.09E + 00 ± 2.90E − 01	1.19E + 01 ± 2.03E + 00	.001	1.26E + 02 ± 8.57E + 01	1.07E + 02 ± 4.07E + 01	.644	2.45E − 02 ± 6.34E − 03	5.28E − 02 ± 1.91E − 02	.644
SHP	NR0B3	6.26E − 01 ± 1.99E − 01	9.22E − 02 ± 2.58E − 02	.027	3.86E + 05 ± 2.30E + 05	3.36E + 05 ± 2.32E + 05	.105	2.33E + 02 ± 4.13E + 01	1.54E + 03 ± 2.07E + 02	.062

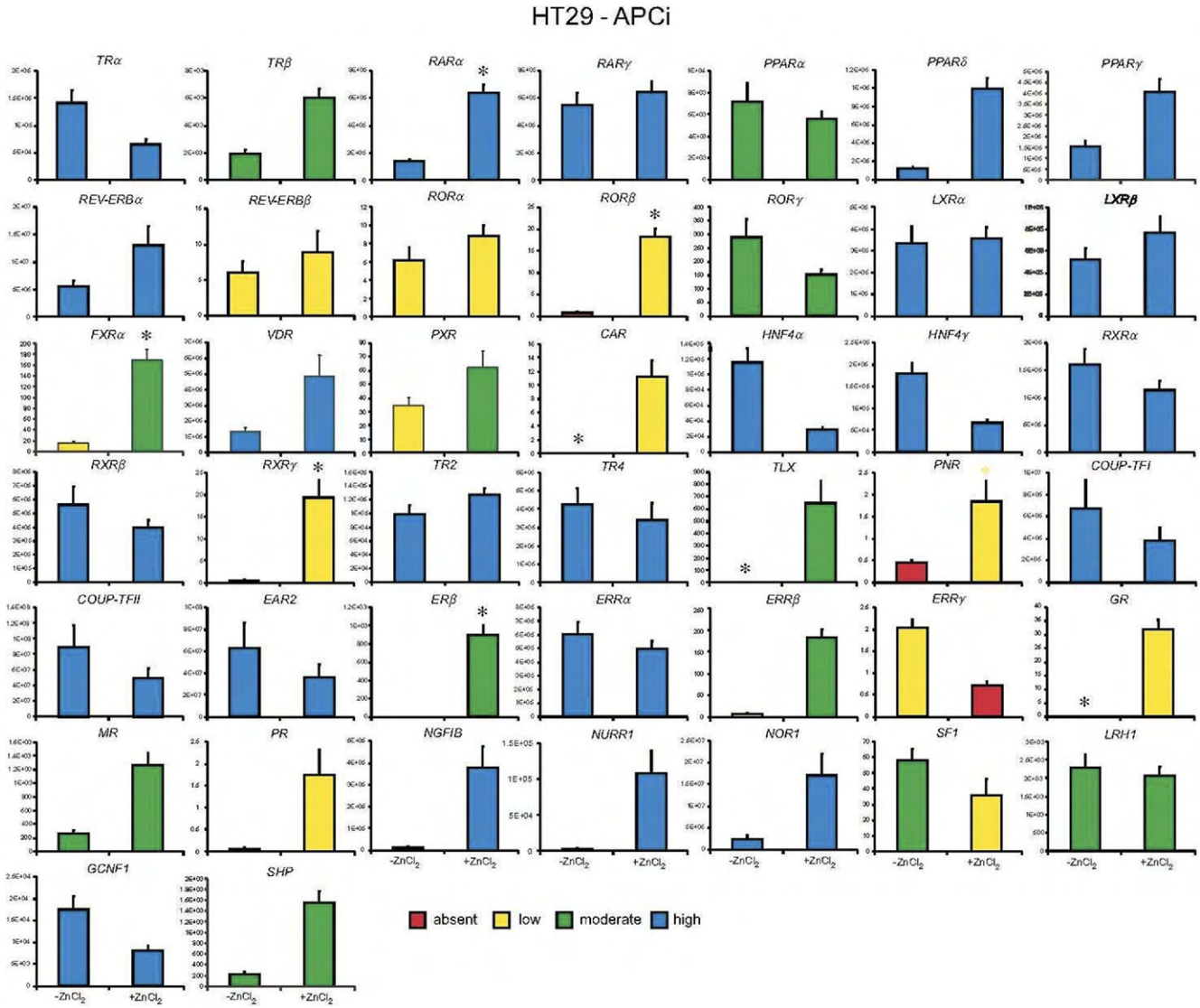

Supplementary Figure 5. Profile of the NR transcriptome in HT29-APC inducible cells. NR expression levels in HT29-APC inducible cells with APC mutated protein (-ZnCl2) were compared with the expression levels after restoring a wild-type APC protein (+ZnCl2). Genes are represented in 4 different colors based on their expression levels (*red*, *yellow*, *green*, and *blue* for absent, low, moderate, and high expression, respectively). Genes that are classified as absent both before and after ZnCl2 are not shown. Values are expressed as relative units and plotted as the mean ± SEM of 6 measurements. *P* values for significant differences are reported in Supplementary Table 2.

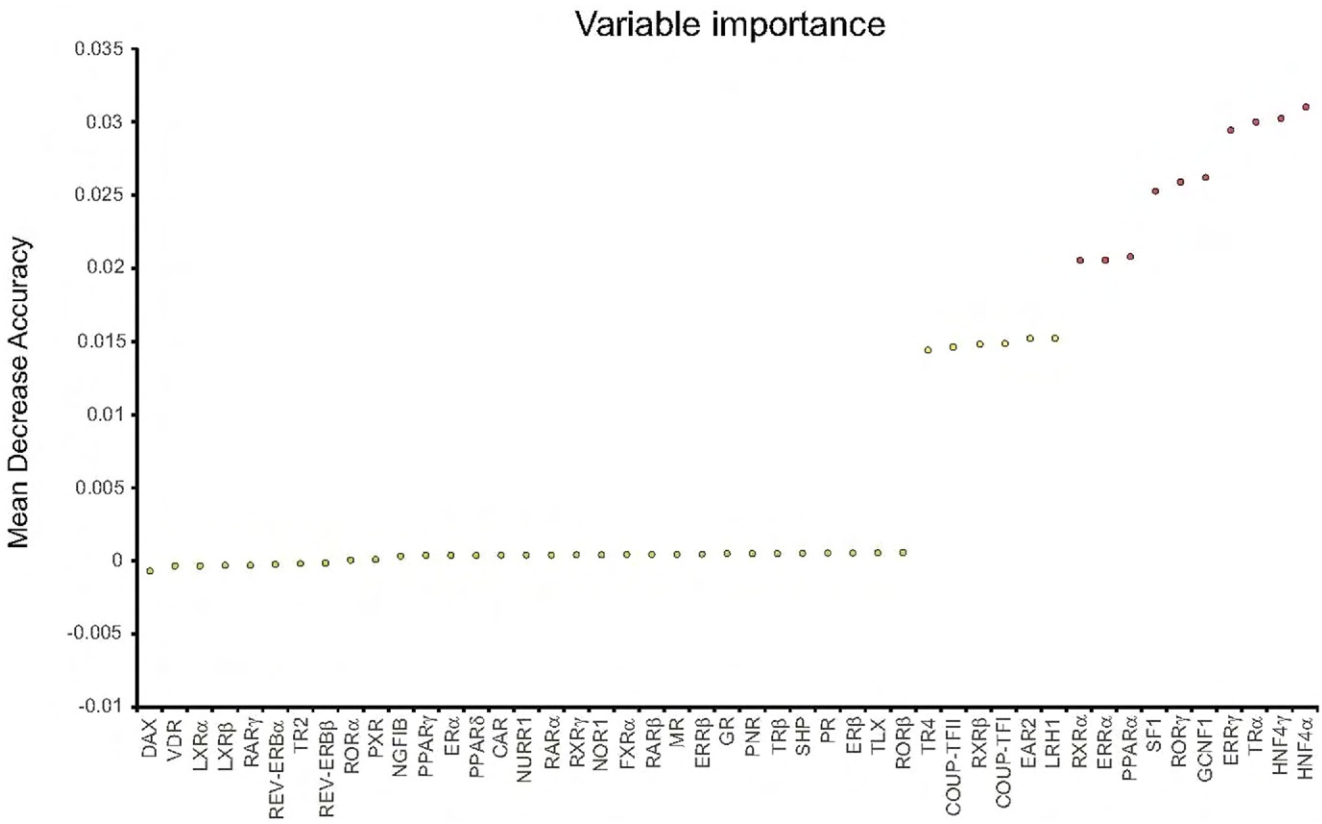

Supplementary Figure 6. Prediction of NR expression modulation in intestinal tumors. Gene clustering to predict a positive or negative change in the APC status from normal mucosa to tumors of FAP patients and $Apc^{Min/+}$ mice was assessed via random forests according to NR expression changes in the HT29-APCi samples (with and without re-expression of a wild-type APC protein). The plot of the variable importance ranking obtained from the random forest displays 5 main clusters of NRs. Those NRs with the lower decrease in accuracy score presented a highly predictive up- or down-regulation change in mRNA abundance from normal mucosa to tumors in human and mouse samples based on the classification clusters obtained in colon cancer cells with and without APC mutation.